Engineering Journal

Second Quarter 2020 | Volume 57, No. 2

Smarter. Stronger. Steel.

Engineering Journal

American Institute of Steel Construction

Dedicated to the development and improvement of steel construction, through the interchange of ideas, experiences and data.

Engineering Journal (ISSN 0013-8029) is published quarterly. Subscriptions: Members: one subscription, $40 per year, included in dues; Additional Member Subscriptions: $40 per year. Non-Members U.S.: $160 per year. Foreign (Canada and Mexico): Members $80 per year. Non-Members $160 per year. Published by the American Institute of Steel Construction at 130 E Randolph Street, Suite 2000, Chicago, IL 60601.

Periodicals postage paid at Chicago, IL and additional mailing offices. **Postmaster:** Send address changes to *Engineering Journal* in care of the American Institute of Steel Construction, 130 E Randolph Street, Suite 2000, Chicago, IL 60601.

Subscriptions: subscriptions@aisc.org, 312.670.2400

Archives: Search at **aisc.org/ej**. Article downloads are free for current members and are avaialable for a nominal fee for non-members.

Investigation on the Performance of a Mathematical Model to Analyze Concentrically Braced Frame Beams with V-Type Bracing Configurations

ALIREZA ASGARI HADAD and PATRICK J. FORTNEY

In memory of Patrick J. Fortney, who passed away in October 2019.

ABSTRACT

The chevron effect and the corresponding mathematical model used to predict the beam shear force and bending moment demands on beams in concentrically braced frames with V- or inverted V-type (also known as chevrons) configurations is studied in this paper. The common analysis approach considers beam span, work point location, and a concentrated force representing the unbalanced vertical forces of the braces while ignoring any local effects resulting from the brace connection geometry. The assumptions and load distribution mechanisms in the connection region that have been discussed in earlier literature are presented, and the performance of the mathematical model based on chevron effect (CE method) is examined by comparing its results with the results of a net vertical force method (NVF) in addition to those obtained by finite element analysis. The analysis procedure recently proposed for beams in chevron concentrically braced frames is used to design the beams in a group of 20 beam-gusset assemblies. The results revealed the presence of the chevron effect in chevron beams. It also showed the CE method is able to estimate the beam maximum shear force and bending moment. Additionally, the stress distribution along the gusset-to-beam interface is studied.

Keywords: beam, shear force, bending moment, concentrically braced frame, chevron, connection, stress distribution.

INTRODUCTION

Braced frames (concentric and eccentric), moment resisting frames, special truss moment frames, and steel plate shear walls are commonly used as lateral-force-resisting systems in steel structures. While new systems such as buckling restrained braced frames are gaining popularity, concentrically braced frames (CBFs) and moment resisting frames (MRFs) are considered as two of the most popular systems among these alternatives (Azad et al., 2017). CBFs have been quite popular since the 1960s mainly because of their economic advantages over the MRFs, particularly in cases where the drift requirements govern the design and higher stiffness and strength are required (Khatib et al., 1988; Nascimbene et al., 2012; Azad et al., 2017). Studies on the seismic response of braced frames progressed slowly until the 1970s. The expansion of offshore oil exploration in regions of seismic risk stimulated analytical and experimental investigations of the inelastic cyclic response of tubular steel–braced structures. At the same time, evidence was accumulating that buildings with braced frames were being damaged during major earthquakes. Such events motivated an increasing number of studies on the inelastic behavior of steel braced frames both analytically and experimentally (Khatib et al., 1988; Bertero et al., 1989; Lee and Lu, 1989; Wallace and Krawinkler, 1989; Tremblay, 2002; Sabelli et al., 2003; Tremblay et al., 2003; Tremblay, 2008). Special concentrically braced frames (SCBFs) were developed after 1988; they are employed in high seismic regions and use a response modification factor, R, to reduce the seismic design force. During large, infrequent earthquakes, SCBFs must sustain cyclic, inelastic tensile yielding and compressive buckling deformation of the brace without significant deterioration of stiffness and resistance for earthquakes exceeding the reduced design force (Sen et al., 2016). Brace buckling and tensile yield are the primary yield mechanisms of the system, which permit the frame to sustain the inelastic deformation and energy dissipation demands needed to provide collapse-prevention performance (Osteraas and Krawinkler, 1989; Naeim, 1998; Roeder et al., 2011; Sen et al., 2016).

For CBFs with buckling braces, the braces are used in opposing pairs to balance the difference in the tensile and compressive capacities. This difference is pronounced in chevron-configured CBFs. In addition to the chevron configuration for CBFs, also known as V- or inverted V-type concentrically braced frames, X-CBFs with braces spanning

Alireza Asgari Hadad, Graduate student, University of Cincinnati, Cincinnati, Ohio. Email: asgariaa@mail.uc.edu (corresponding)

Patrick J. Fortney, Associate Professor-Educator, University of Cincinnati, Cincinnati, Ohio.
In memory of Patrick J. Fortney, who passed away in October 2019.

Paper No. 2018-07R

two consecutive floors meeting at one point in the middle beam were also used in CBFs. An inventory of older CBF buildings shows that the chevron brace configuration was common (Zhang et al., 2011; Sloat, 2014; Sen et al., 2016). This is logical because chevron bracing accommodates a wide range of architectural elements, including doors and windows, and fewer brace connections with respect to X-CBFs (Sen et al., 2016; Costanzo et al., 2017). Chevron-braced bays were found to fail in one of two mechanisms: (1) A weak beam mechanism where the buckling of the compression brace causes an unbalanced force to be applied on the beam and subsequently the formation of plastic hinges in the beam. Weak beams lead to considerable plastification in columns, beams, and braces, irrespective of brace slenderness. Slender braces increase the ductility demand in all remaining members, and rarely yield in tension. (2) A strong beam mechanism where buckling of the compression brace is followed by yielding of the tension brace, the beam being sufficiently strong to remain elastic despite the vertical unbalanced force applied to it by the braces at mid-span. Chevron-braced frames with strong beams and weak braces exhibit a more uniform distribution of yielding with height than frames with weak beams and strong braces (D'Aniello et al., 2015). It is not evident from the data in the literature which collapse mechanism is preferable. The weak beam mechanism concentrates the energy dissipation in the beams that are better energy dissipators than the braces. However, it causes a deteriorating force deformation curve, which leads to more energy dissipation demand. The strong beam mechanism provides a trilinear force deformation characteristic that is believed by many to be an ideal force deformation characteristic. On the other hand, it concentrates the energy dissipation in the braces (the least capable elements) and may require unreasonably stiff and strong beams. In addition, it increases the maximum column compression and hence the danger of column buckling. This is a very undesirable situation in that it might lead to column failure, soft-story formation, or incremental collapse (Roeder and Popov, 1978; Rega and Vestroni, 1984; Shen et al., 2015). The mentioned uncertainties regarding the demands on the beam in chevron CBFs with a V- or X-bracing configuration jeopardize the support of the floor and thus make chevron V- and X-bracing undesirable bracing configurations (ASCE, 1998).

In addition to the system behavior in CBFs, brace connection analysis and design and calculation of the connection interface forces have been a subject for several numerical and experimental studies (Thornton, 1984; Astaneh-Asl et al., 1985; Bjorhovde and Chakrabarti, 1985; Richard, 1986; Willibald et al., 2006; Shaw et al., 2010; Wigle and Fahnestock, 2010). The uniform force method (UFM) is a popular method typically used to distribute brace forces through the corner connections (Thornton, 1991). However, this method is limited to connections where braces are framed to a beam-column joint. There is very little published work on how to distribute forces in other types of brace configuration. Fortney and Thornton (2015; 2017) studied CBFs with V- and inverted V-type brace configurations. They discussed the behavior of frame beams through a phenomenon called the chevron effect and developed a mathematical method to, initially, determine an admissible distribution of forces acting on the beam-to-gusset interface and, secondly, determine the beam shear force and bending moment in the connection region. It is worth noting that the chevron effect model does not consider any stiffening effect of the gusset plate for the beam. This assumption relies on the results of several experimental tests revealing the out-of-plane bending of the gusset plate when the compression brace buckles (Zhang et al., 2011; Lumpkin et al., 2012; Okazaki et al., 2012; Hsiao et al., 2013; Salawdeh et al., 2017). The mentioned mathematical model will be discussed, and its performance will be studied and compared with finite element model results in the following sections.

MATHEMATICAL MODEL FOR CHEVRON EFFECT

The chevron effect is a phenomenon that affects the demands on the frame beam imparted by the distribution of forces at the beam/gusset plate interface. The influence of these interface forces on the beam demands was initially introduced by Fortney and Thornton (2015). The chevron effect is present in CBFs with V- and inverted V-type brace configurations where braces are connected to the frame beam with a gusset plate. The net vertical force (NVF) method is the common method used to analyze the frame beam in such braced frames. However, this method only considers the center line of the columns, beams, and braces and applies the summation of the vertical components of the brace forces to the work point (the point in which the center lines of the braces meet the centerline of the beam) as concentrated load. Fortney and Thornton (2015) developed a mathematical model assuming a uniform distribution of connection interface forces and moments to calculate the shear force and bending moment on the beam. They showed that the presence of a gusset plate influences the force distribution in the connection region and referred to this phenomenon as the chevron effect. Fortney and Thornton (2017) showed the chevron effect results in localized beam shear and moment demands on the frame beam that are not captured by the NVF. Figure 1 presents the chevron effect and the difference between the results of the mathematical model (CE method) and the NVF method for the case in which the tension and compression braces have equal forces (i.e., zero NVF).

The CE method proposed by Fortney and Thornton (2015;

2017) to analyze the beam in a chevron brace frame does not consider the gusset plate as a stiffening element for the beam. So the flexural deformation of the beam is not influenced by the gusset plates in the connection region. This assumption is based on the instability of the gusset plate at the free edges and the out-of-plane deformation of the gusset plate during brace buckling. The out-of-plane behavior of the gusset plate is observed in several studies. Zhang et al. (2011) studied nine inverted V-braces (W-shapes) and their gusset plate connections under inelastic cyclic loading to define the hysteretic behavior of the assemblies. As can be seen in Figure 2, even the presence of stiffener plates does not impede the out-of-plane response of the gusset plate [see Figure 2(b)].

While the cyclic and monotonic response of isolated components such as braces and gusset plates has been the subject of several studies, the seismic response of two three-story SCBFs was studied to investigate the performance of their structural components when the components work interactively (Lumpkin et al., 2012). The gusset plate rotation and out of plane buckling phenomenon was also observed in this study (see Figure 3). Similar observations are reported by other researchers (Okazaki et al., 2012; Hsiao et al., 2013; Salawdeh et al., 2017).

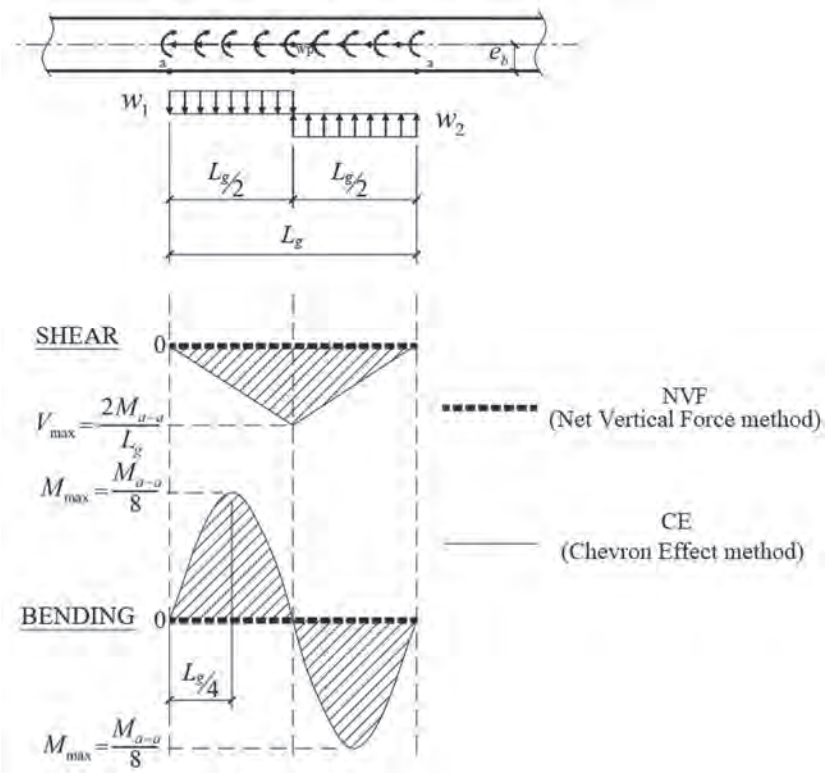

Fig. 1. The chevron effect—beam shear and moment (Fortney and Thornton, 2017).

(a) Without stiffener *(b) With stiffener*

Fig. 2. Deformation of gusset plates (Zhang et al., 2011).

TEST MATRIX

To evaluate the performance of the CE method, 20 gusset-beam assemblies are designed. Each assembly consists of a beam and either one or two gussets representing the two types of studied CBFs: a chevron (Vb) or X-bracing (Xb) configuration, respectively. The gusset is connected to the beam with two-sided fillet welds.

In order to provide enough freedom for the braces to buckle in real practice, a clearance must be provided between the end of the brace-to-gusset weld and the beam-to-gusset interface. Two values of clearances (2.0 in. and 8.0 in.) are considered in the models in order to evaluate the effect of the clearance distance on the stress distribution of the welded connection interface. The 2.0-in. clearance is assumed to represent a clearance that might be used when the braces frame to the bottom side of a beam. The 8.0-in. clearance is assumed to represent a clearance that might be used when a gusset frames to the top side of a beam (e.g., if one wanted the end of the brace to clear a floor slab). Models identified with an uppercase L, such as "M1 L", are the models with the 8.0-in. clearance.

Three types of loads are considered in the design of the gussets and the beam-to-gusset welds: (1) equal tension and compression brace forces (Equation l); (2) mechanism load (Mec), which is the expected tensile strength of the tension brace and the expected buckling strength of the compression brace (in the case of X-bracing configuration, it will be the yield of two braces on a same line and buckling of the other two braces on the other line); and (3) the expected post-buckling strength of the compression brace (Pst) and the expected tensile strength of the tension brace. The brace forces are calculated using Equations 1–3 as required in AISC *Seismic Provisions* Section F2.6c (AISC, 2016).

$$P_{tension} = R_y F_y A_g \quad (1)$$

$$P_{compression} = 1.14 F_{cre} A_g \quad (2)$$

$$P_{post\text{-}buckling} = 0.3 P_{compression} \quad (3)$$

For sizing the beam, the maximum shear force and bending moment are obtained based on the CE method. The most economic (lightest) section is selected from Part 1 of the AISC *Steel Construction Manual* (AISC, 2017). Figure 4 shows the process of designing the beam using the CE method and compares it with the NVF method. The main difference between the two methods is that the NVF method is not dependent on the beam size and gusset geometry whereas the CE method is. Therefore, the CE method is an iterative process whereas the NVF method is not. The governing limit state for each beam used in each assembly is provided in Table 1.

Gusset thickness is determined based on eight limit states, including:

1. Tension along the brace line based on Whitmore section.
2. Compression along the brace line based on the Whitmore section.
3. Normal (axial) force to section a-a.
4. Shear force along section a-a.
5. Bending moment on section a-a.
6. Normal (axial) force to section b-b.
7. Shear force along section b-b
8. Bending moment on section b-b.

Figure 5 shows the design parameters.

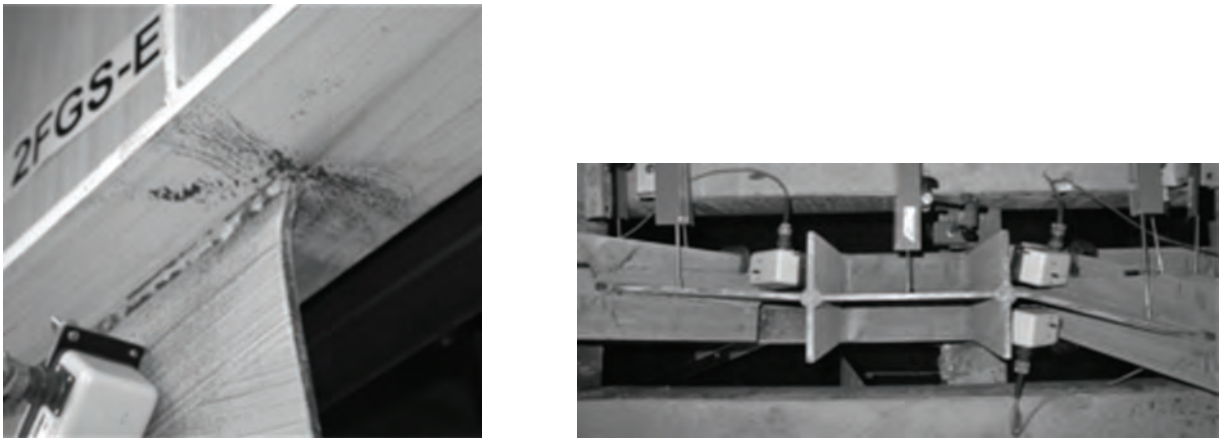

(a) *(b)*

Fig. 3. Mid-span gusset rotation due to brace buckling (Lumpkin et al., 2012).

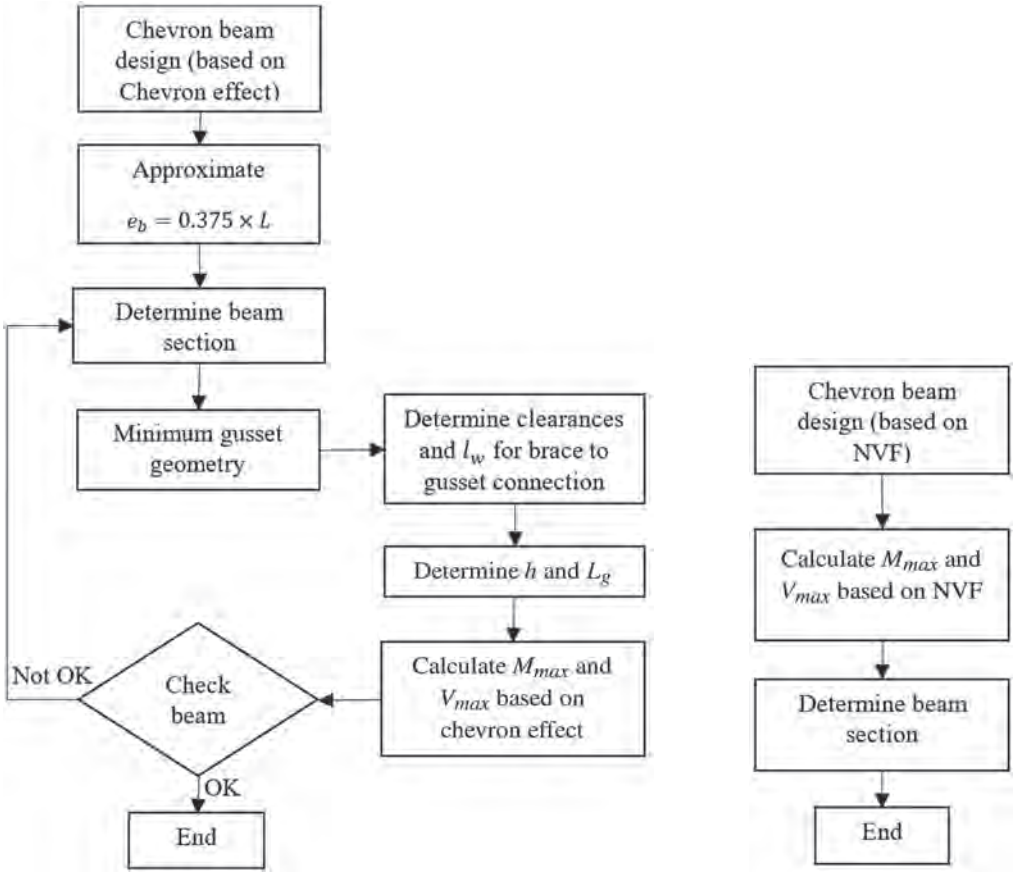

(a) Design based on CE *(b) Design based on NVF*

Fig. 4. Comparison of chevron beam design methods.

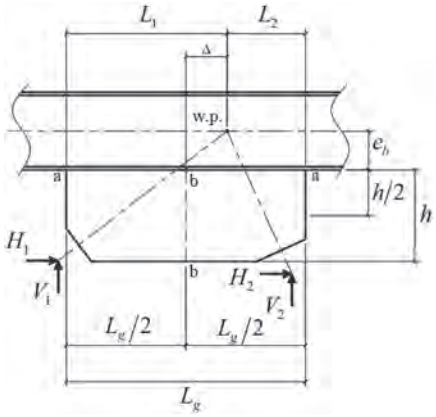

Fig. 5. Design parameters (Fortney and Thornton, 2015).

Table1. List of FEA Models with Design Details

No.	Model	Clearance (in.)	Load	Beam	Beam Limit State	t_{gusset} (in.)	Gusset Limit State	*D* (in.)	Geometry (in.)				Type
									H	*a*	*b*	Δ	
1	M1	2	Eql	W14×26	V	3/8	C	3/16	150	150	150	0	Vb
2	M1 L	8	Eql	W12×26	V	1/2	C	1/8	150	150	150	0	Vb
3	M2	2	Eql	W18×65	V	3/8	C	3/16	150	150	150	0	Xb
4	M2 L	8	Eql	W16×50	V	1/2	C	1/8	150	150	150	0	Xb
5	M3	2	Mec	W30×108	M	7/16	$A_{b\text{-}b}$	3/16	150	150	150	0	Vb
6	M3 L	8	Mec	W30×108	M	7/16	T	3/16	150	150	150	0	Vb
7	M3 Pst	2	Pst	W30×108	M	7/16	$A_{b\text{-}b}$	3/16	150	150	150	0	Vb
8	M3 L Pst	8	Pst	W30×108	M	7/16	T	3/16	150	150	150	0	Vb
9	M4	2	Mec	W24×84	V	7/16	T	3/16	150	150	150	0	Xb
10	M4 L	8	Mec	W21×62	V	7/16	T	3/16	150	150	150	0	Xb
11	M4 Pst	2	Pst	W24×84	V	7/16	T	3/16	150	150	150	0	Xb
12	M4 L Pst	8	Pst	W21×62	V	7/16	T	3/16	150	150	150	0	Xb
13	M5	2	Mec	W24×76	V	7/16	T	3/16	150	120	180	4	Xb
14	M5 L	8	Mec	W21×55	V	7/16	T	3/16	150	120	180	5	Xb
15	M5 Pst	2	Pst	W24×76	V	7/16	T	3/16	150	120	180	4	Xb
16	M5 L Pst	8	Pst	W21×55	V	7/16	T	3/16	150	120	180	5	Xb
17	M6	2	Mec	W24×84	V	7/16	T	1/4	180	144	156	1	Xb
18	M6 L	8	Mec	W21×62	V	1/2	T	1/4	180	144	156	2	Xb
19	M6 Pst	2	Pst	W24×84	V	7/16	T	1/4	180	144	156	1	Xb
20	M6 L Pst	8	Pst	W21×62	V	1/2	T	1/4	180	144	156	2	Xb

Eql: Equal tension and compression loading
Mec: Mechanism (buckling) loading
Pst: Post-buckling loading
$A_{b\text{-}b}$: Axial load on gusset section b-b
C: Compression
T: Tension
R: Rectangular
W: Whitmore
H: Story height
V: Shear
M: Moment (bending)
Vb: Chevron bracing configuration
Xb: X bracing configuration
a: Distance from work-point to left beam end
b: Distance from work-point to right beam end
Δ: Horizontal eccentricity
t_{gusset}: Gusset thickness

FINITE ELEMENT MODELS:

Abaqus 6.13 (Simulia, 2013) is employed to model and analyze the gusset-beam assemblies (listed in Table 1) and evaluate beam shear force and bending moment. An eight-node linear brick element is used for all parts in the models. An elastic perfectly plastic material model is used for all parts: ASTM A992 for the beams ($F_y = 50$ ksi), ASTM A529 Gr. 50 for the gussets ($F_y = 50$ ksi), and E70 ($F_u = 70$ ksi) for the welds. Two-sided fillet welds are used to connect the gusset(s) to the beam. Different mesh sizes were studied for each of the parts to find the appropriate mesh size. The mesh size study is summarized in Figure 6. The selected mesh sizes are 1 in. for the beam, 0.3 in. for the gusset, and 0.2 in. for the weld materials.

ANALYSIS RESULTS

The shear force and bending moment diagrams of the beams were extracted from the finite element analysis (FEA) and plotted to compare the prediction of the CE and NVF methods to that of the FEA. Because the maximum beam shear force and bending moment are the important values in designing the beam section, a summary of the maximum values is reported in Table 2. To discuss and compare the results in more detail, all models are categorized into four groups based on the summation of the braces' vertical forces and the number of gusset plates used in each model:

1. Group1: $\Sigma V_T = 0$; gusset plate on one side of the beam
2. Group 2: $\Sigma V_T = 0$; gusset plate on both sides of beam
3. Group 3: $\Sigma V_T \neq 0$; gusset plate on one side of beam
4. Group 4: $\Sigma V_T \neq 0$; gusset plates on both sides of beam

The results of the analyses for each group are presented in the following sections.

Group 1: Summation of Vertical Forces = Zero; Single Gusset Plate

Because the summation of vertical forces is zero in this group, the NVF method does not predict any shear force and bending moment on the beam. However, due to the presence of the gusset, there is a shear force and bending moment on the beam due to the chevron effect, which is also observed in the FEA results. As can be seen in Table 3, the CE method predicts the maximum beam shear force and bending moment with values close to the FEA values. On average, the maximum beam shear force derived by CE method is 20% (1.22) larger than that of the FEA, and the maximum beam moment is approximately equal the FEA value (0.96). The distribution of beam shear force and bending moment for all methods is plotted in Figure 7 for model M1.

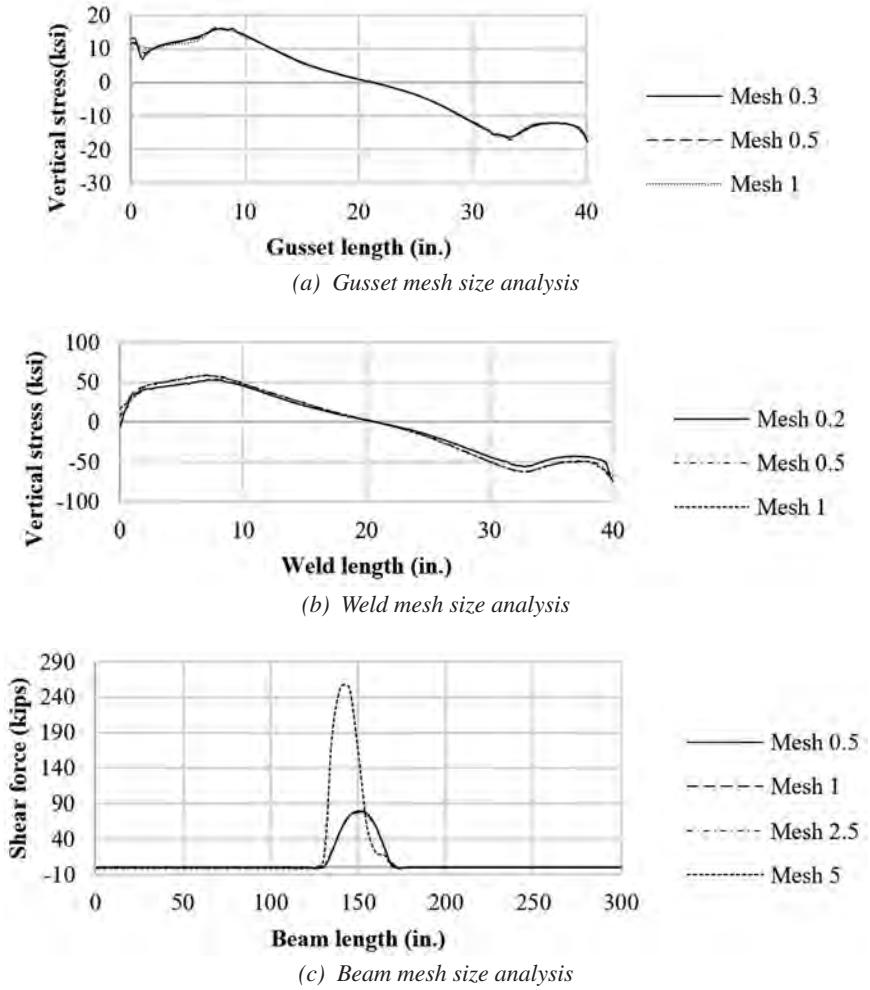

(a) Gusset mesh size analysis

(b) Weld mesh size analysis

(c) Beam mesh size analysis

Fig. 6. Mesh size determination analysis for different parts.

Table 2. Summary of Results							
		CE		NVF		FEA	
No.	Model	V_{max} (kips)	M_{max} (kip-in.)	V_{max} (kips)	M_{max} (kip-in.)	V_{max} (kips)	M_{max} (kip-in.)
1	M1	93.4	244	0.00	0.00	79.4	256
2	M1 L	66.4	214	0.00	0.00	52.2	219
3	M2	226	651	0.00	0.00	183	228
4	M2 L	165	577	0.00	0.00	126	88.6
5	M3	169	8,130	56.7	8430	147	6,720
6	M3 L	144	7,920	56.7	8430	127	6,330
7	M3 Pst	132	13,600	99.1	14,800	123	11,800
8	M3 L Pst	112	13,300	99.1	14,800	113	11,200
9	M4	305	1,110	0.00	0.00	248	358
10	M4 L	227	964	0.00	0.00	181	107
11	M4 Pst	236	853	0.00	0.00	191	278
12	M4 L Pst	176	742	0.00	0.00	139	86.0
13	M5	313	5730	43.9	5,220	251	4,090
14	M5 L	224	5,520	43.9	5,220	196	4,090
15	M5 Pst	241	4,410	33.9	4,020	192	3,150
16	M5 L Pst	163	4,230	33.9	4,020	149	3,150
17	M6	309	1,870	6.81	980	259	813
18	M6 L	225	1,720	6.81	980	187	783
19	M6 Pst	238	1,440	5.24	754	200	624
20	M6 L Pst	173	1,330	5.24	754	143	603

Table 3. Summation of Vertical Forces = Zero; Single Gusset Plate							
		CE/FEA		NVF/FEA		NVF/CE	
No.	Model	V_{max} (kips)	M_{max} (kip-in.)	V_{max} (kips)	M_{max} (kip-in.)	V_{max} (kips)	M_{max} (kip-in.)
1	M1	1.18	0.954	0.000	0.000	0.000	0.000
2	M1 L	1.27	0.977	0.000	0.000	0.000	0.000
Average		1.23	0.966	0.000	0.000	0.000	0.000

Group 2: Summation of Vertical Forces = Zero; Double Gusset Plates

Similar to the first group's models, the summation of vertical forces is zero in this group, and thus the NVF does not predict any beam shear force and bending moment. As presented in Table 4, the CE method predicts a beam maximum shear force approximately 20% larger than that of the FEA. There is a big difference, however, between the maximum bending moment predicted by CE method versus the one in the FEA; the CE maximum bending moment is, on average, 5.5 times the FEA value. The difference is due to the presence of double gusset plates and the unavoidable suggestion of the FEA to stiffen the beam section with the gusset plates. It influences the beam flexural deformation, which leads to different beam bending moment values. The mentioned view point on the gusset plate(s) opposes the CE method that assumes (based on the discussed experimental observations) the gusset plate(s) does not stiffen up the beam section and thus does not have any impact on the magnitude of the beam bending moment. Regardless of the mentioned issue, the CE method can yet be a useful tool in the analysis and designing of such beams because the shear force is the governing limit state in selecting the beam section and the NVF method is not able to predict any shear force demand on the beam. The analysis results of model M2 is plotted in Figure 8 as an example.

(a) Model geometry

(b) Deformed shape

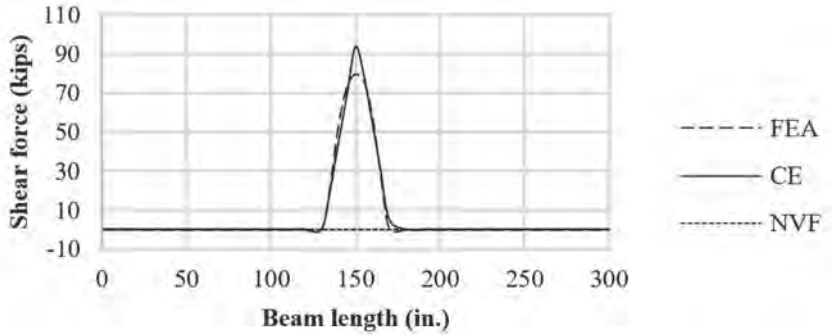

(c) Beam shear force diagram

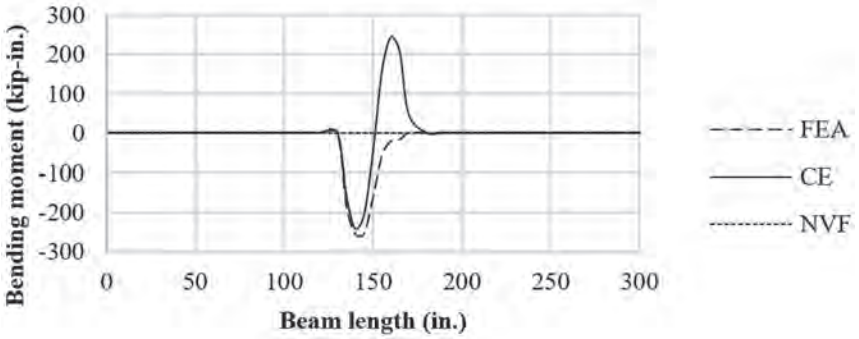

(d) Beam bending moment diagram

Fig. 7. Model M1 results.

Table 4. Summation of Vertical Forces = Zero; Double Gusset Plates							
		CE/FEA		NVF/FEA		NVF/CE	
No.	Model	V_{max} (kips)	M_{max} (kip-in.)	V_{max} (kips)	M_{max} (kip-in.)	V_{max} (kips)	M_{max} (kip-in.)
3	M2	1.24	2.85	0.000	0.000	0.000	0.000
4	M2 L	1.31	6.51	0.000	0.000	0.000	0.000
9	M4	1.23	3.10	0.000	0.000	0.000	0.000
10	M4 L	1.26	9.02	0.000	0.000	0.000	0.000
11	M4 Pst	1.24	3.07	0.000	0.000	0.000	0.000
12	M4 L Pst	1.27	8.64	0.000	0.000	0.000	0.000
Average		1.26	5.53	0.000	0.000	0.000	0.000

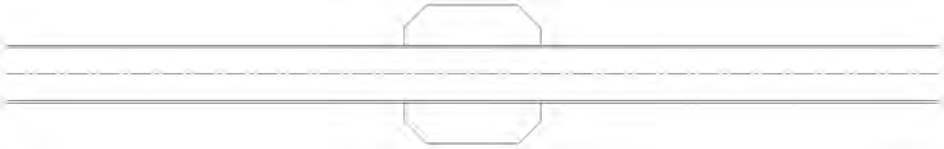

(a) Model geometry

(b) Deformed shape

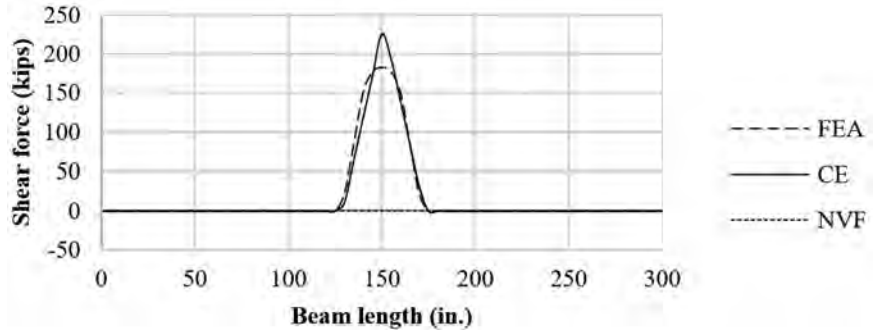

(c) Beam shear force diagram

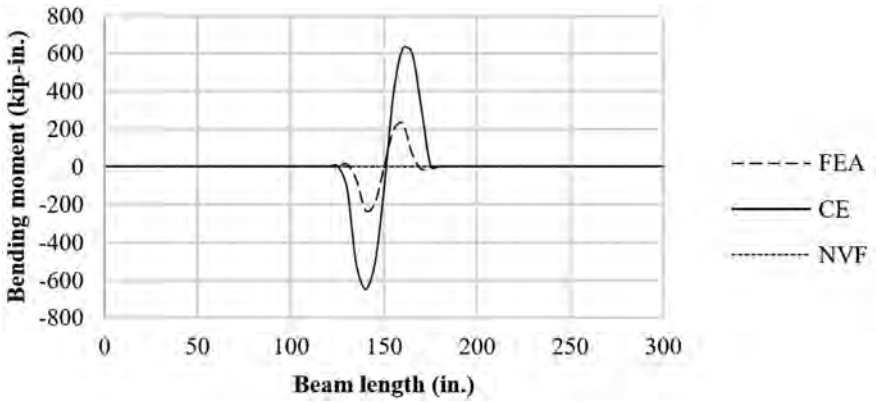

(d) Beam bending moment diagram

Fig. 8. Model M2 results.

Table 5. Summation of Vertical Forces ≠ Zero; Single Gusset Plate							
		CE/FEA		NVF/FEA		NVF/CE	
No.	Model	V_{max} (kips)	M_{max} (kip-in.)	V_{max} (kips)	M_{max} (kip-in.)	V_{max} (kips)	M_{max} (kip-in.)
5	M3	1.16	1.21	0.387	1.26	0.335	1.04
6	M3 L	1.13	1.25	0.447	1.33	0.395	1.06
7	M3 Pst	1.07	1.16	0.803	1.25	0.752	1.08
8	M3 L Pst	0.992	1.19	0.875	1.32	0.881	1.11
Average		1.09	1.20	0.628	1.29	0.591	1.07

Group 3: Summation of Vertical Forces ≠ Zero; Single Gusset Plate

Based on the results in Table 5, the NVF method can predict the beam maximum bending moment in the models in which the summation of the vertical forces is not zero, but this method does not predict the beam maximum shear force. On the other hand, the CE method estimates a beam maximum shear force; approximately corresponding to the FEA (1.09) and bending moment 20% larger than FEA results. Thus, the CE method can be considered as a more versatile tool in analyzing chevron beams. The results of model M3 in this group is plotted in Figure 9.

Group 4: Summation of Vertical Forces ≠ Zero; Double Gusset Plates

Due to the presence of double gusset plates and the discussed issue regarding the stiffening influence of the gusset plates on the beam section, the CE method predicts the maximum beam moment on average 80% greater than that of the FEA. Because the beam maximum shear force is the determinative limit state in designing the X-bracing chevron beams (double gusset plate), and the CE method can estimate the maximum beam shear force with 20% difference in comparison to the FEA; the CE method can be used in analyzing such beams. Note that the NVF method does not

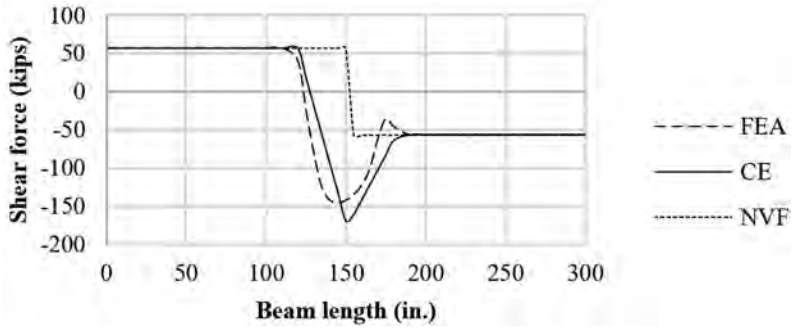

(a) Beam shear force

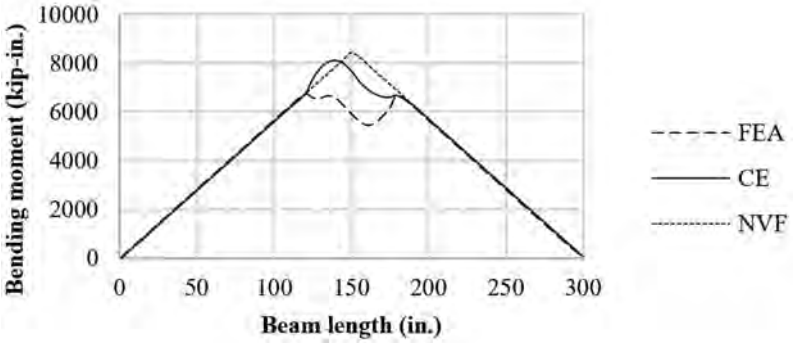

(b) Beam bending moment

Fig. 9. Model M3 results.

Table 6. Summation of Vertical Forces ≠ Zero; Double Gusset							
		CE/FEA		NVF/FEA		NVF/CE	
No.	Model	V_{max} (kips)	M_{max} (kip-in.)	V_{max} (kips)	M_{max} (kip-in.)	V_{max} (kips)	M_{max} (kip-in.)
13	M5	1.25	1.40	0.175	1.28	0.141	0.912
14	M5 L	1.15	1.35	0.225	1.28	0.196	0.947
15	M5 Pst	1.25	1.40	0.176	1.28	0.141	0.912
16	M5 L Pst	1.09	1.34	0.227	1.28	0.208	0.950
17	M6	1.19	2.30	0.026	1.21	0.022	0.524
18	M6 L	1.21	2.20	0.037	1.25	0.030	0.569
19	M6 Pst	1.19	2.31	0.026	1.21	0.022	0.524
20	M6 L Pst	1.21	2.20	0.037	1.25	0.030	0.569
Average		1.19	1.81	0.116	1.25	0.099	0.738

estimate the maximum beam shear force in such models (see the maximum shear ratios in Table 6). Model M5 results are plotted in Figure 10.

PERFORMANCE OF THE CE METHOD IN THE CASE OF FLAT BAR GUSSETS

As discussed earlier, the FEA suggests that the gusset plate(s) stiffen the beam influencing the flexural deformation of the beam and thus the beam bending moment values. In order to remove this influence, model M1 is reconsidered with one difference; the rectangular gusset plate is replaced with a couple of flat bar gusset plates. The new model's geometry and the analysis results are shown in Figure 11. According the beam shear force and bending moment results, the CE method correlates very well with the FEA when the stiffening influence of the gusset plate on the beam section is removed. As such, the assumption of uniformly distributed

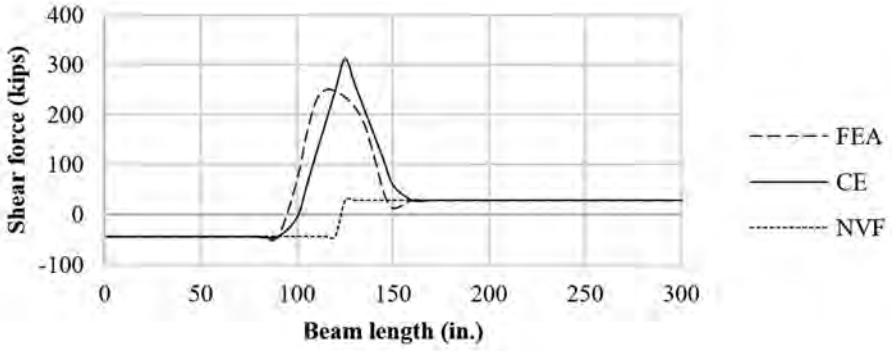

(a) Beam shear force

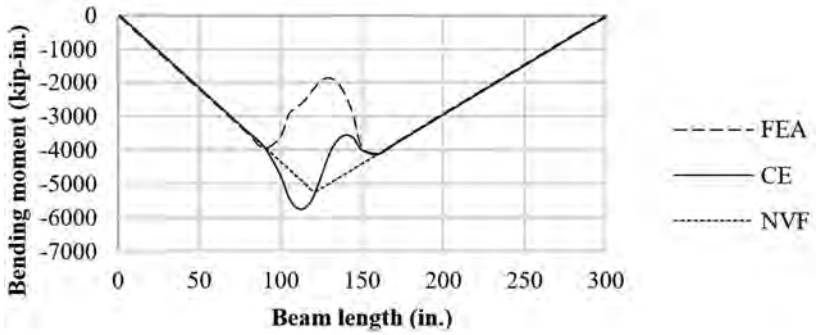

(b) Beam bending moment

Fig. 10. Model M5 results.

loads acting at the flat bar-beam interfaces is a valid assumption for flat bar gusset connections as well.

UNIFORM VERSUS NONUNIFORM STRESS DISTRIBUTION:

One of the common issues in brace connections is the uneven stress distribution across the gusset edge (Richard, 1986). In the case of a bracing connection welded to the flange of a member, which has significantly more rigidity than a connection to the web, the potential inability of the system to accommodate force distribution was observed (Hewitt and Thornton, 2004). The development of a peak stress induced at some point across the welded connection might cause the weld to fail at the point where the stress is concentrated, causing an unzipping of the weld and a progressive failure of the welded connection (Hewitt and Thornton, 2004). Such a phenomenon has been confirmed in experimental studies as well. See Figure 12 as an example (Lumpkin et al., 2012). To solve this issue, Richard (1986) considered the ratio of peak over average of the stress distribution at the edges of the studied gussets. In response to the Richard (1986) study, AISC introduced a weld ductility factor, equal to 1.4, that was intended to allow for adequate stress redistribution in the weld across the interface. That factor was subsequently reduced to 1.25 (Hewitt and Thornton, 2004).

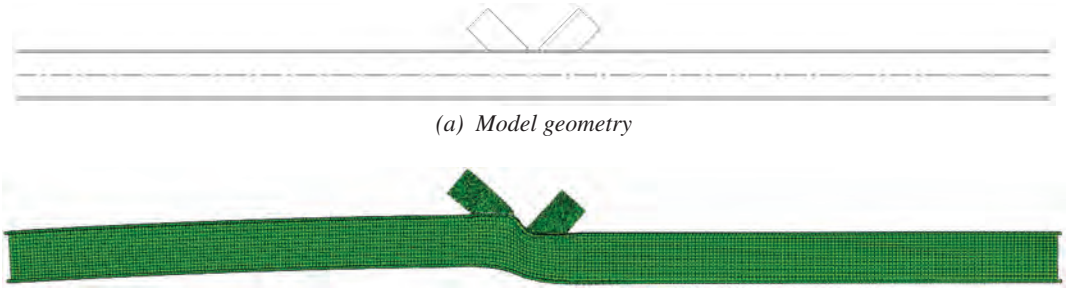

(a) Model geometry

(b) Deformed shape

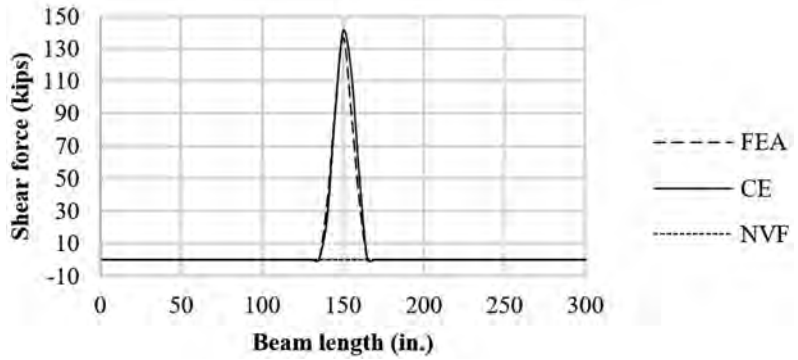

(c) Beam shear force diagram

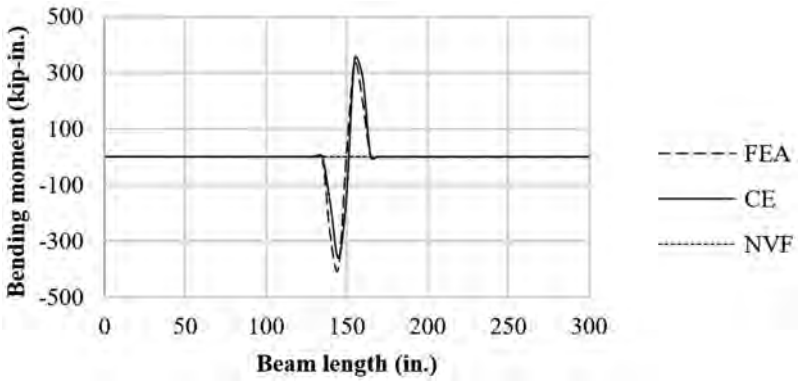

(d) Beam bending moment diagram

Fig. 11. Model M1 with flat bar gusset plates results.

Stress concentration at the edges of the gusset(s) to the weld interface was observed in all finite element models studied in this research. Figure 13 shows a sample presenting the stress concentration at the left edge of the gusset-to-weld connection. In order to check the the stress distrubution along the gusset-to-weld connection region, a section cut is considered along the bottom of the gusset plate (above the fillet weld), and the vertical stress distribution at the section cut is studied. Finally, the peak over average ratio of the vertical stress distribution along the gusset to weld connection region is evaluated for all of the models.

Figure 14 shows the variation of peak to average ratio in 67 welded gusset connections. These values are also tabulated in Table 7. In Table 7, the ratios are given for the left and right half (compression and tension zones) of the gussets. The average of all ratios is 2.38, and the standard deviation is 0.63. These results show that the 1.4 ductility factor originally required for the corner gusset plates should be increased to a larger value (approximately 3) in the case of middle gusset plates used in chevron configuration. Another possible approach to solve this problem is to design the welds based on the shear strength of the gusset plate. Further studies with regard to the determination of the ductility factor for the case of chevron gusset plate connections are recommended by the authors.

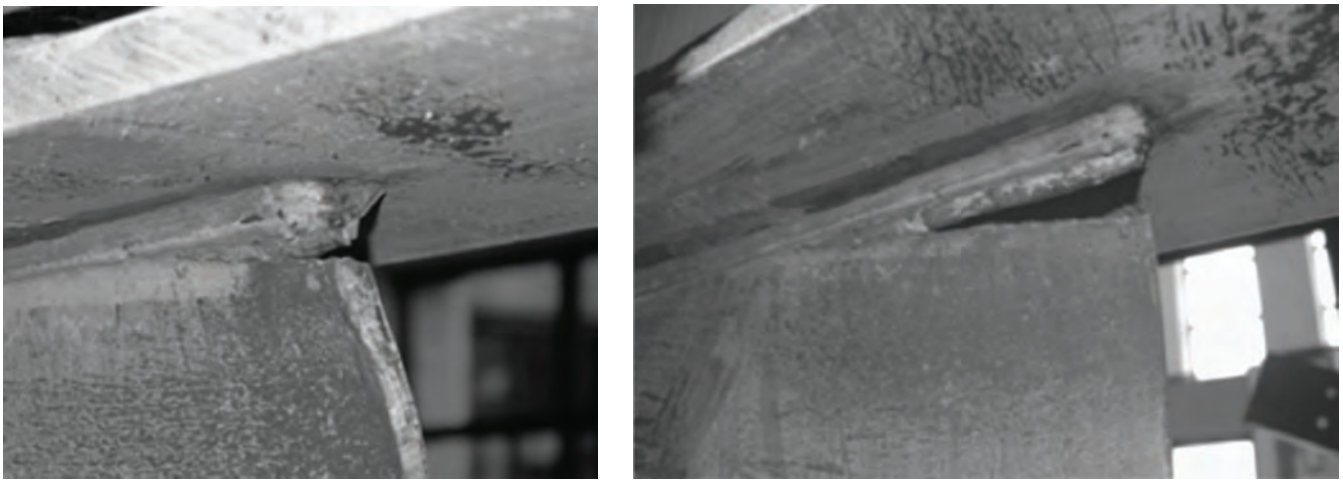

(a) During the test *(b) End of the test*

Fig. 12. Weld tearing at corner gusset plate (Lumpkin et al., 2012).

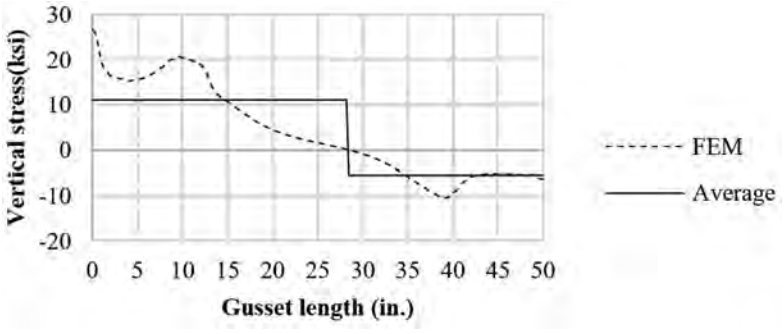

Fig. 13. Vertical stress distribution at gusset to weld interface, model M6.

Table 7. Vertical Stress Distribution Ratios					
		Top Gusset		Bottom Gusset	
		Peak/Average		Peak/Average	
No.	Model	Left Half	Right Half	Left Half	Right Half
1	M1	1.74	1.89	—	—
2	M1 L	3.87	2.13	—	—
3	M2	1.96	2.01	1.95	1.93
4	M2 L	2.18	2.16	2.33	2.23
5	M3	2.10	2.61	—	—
6	M3 L	2.54	1.88	—	—
7	M3 Pst	1.99	1.79	—	—
8	M3 L Pst	2.36	1.41	—	—
9	M4	2.24	2.03	2.13	2.12
10	M4 L	2.03	2.27	2.19	2.44
11	M4 Pst	2.43	3.76	2.32	3.90
12	M4 L Pst	2.26	2.70	2.35	2.84
13	M5	2.18	2.80	2.32	2.73
14	M5 L	2.70	1.90	1.90	2.99
15	M5 Pst	2.68	2.26	2.34	3.36
16	M5 L Pst	3.22	1.65	1.88	2.49
17	M6	2.38	1.94	2.14	2.53
18	M6 L	2.58	1.34	1.71	3.42
19	M6 Pst	2.44	1.93	2.23	5.07
20	M6 L Pst	3.34	—	2.55	1.91

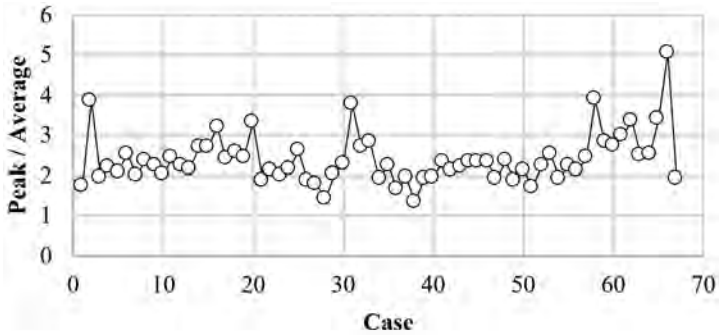

Fig. 14. Variation of peak over average vertical stress ratio in all assemblies.

CONCLUSION

The chevron effect is a phenomenon that occurs in the frame beams of CBFs with chevron V- and inverted V-bracing configurations due to the presence of gusset plate(s). This phenomenon was introduced in earlier literature, and a mathematical model was developed to generate an admissible force distribution in the chevron gusset connection to obtain beam shear force and bending moment with the inclusion of the chevron effect. The work reported in this paper considered 20 beam-gusset assemblies connected by fillet welds. To check the performance of the mathematical model (CE method), the authors used finite element analysis (FEA) to investigate the beam shear force and bending moment of all models.

The FEA results clearly revealed the presence of the chevron effect in the beam shear force and bending moment diagrams. The net vertical force (NVF) method, which has been commonly used in analyzing chevron beams, was not able to capture the chevron effect and could not estimate the maximum beam shear force accurately in all models, while the CE method could capture the chevron effect. On average, the maximum beam shear force estimated by CE method is approximately 20% higher of that in the FEA results. Thus, the CE method can always estimate the beam shear force with an acceptable conservatism.

Due to the out-of-plane behavior of the gusset plate, the CE method does not consider the gusset plate(s) as a stiffening element for the beam section. However, the FEA stiffens the beam section by the gusset plate(s), which influences the beam flexural deformation and thus the value of bending moment. The mentioned issue caused the difference between the CE method and the finite element model bending moment results, specifically for models with double gusset plates. On average, the ratio between the CE maximum bending moment and that of the FEA analysis is 2.4. However, because the maximum beam shear force is the governing limit state in cases with X-bracing configurations (double gusset plates), the CE method reasonably predicts the maximum beam shear force in such models and can be a useful tool in designing all types of chevron brace frame beams. If one can reasonably ensure that the gusset will experience no out-of-plane deformations, a rational analysis of the beam that includes the gusset stiffening effects may be reasonable.

The stress concentrations at the ends of the gusset-to-beam welds, caused local failure at the weld terminations. To avoid this local failure, the ratio of peak over average of the vertical stress distribution along the gusset to weld connection interface is calculated and studied. The results showed the ductility factor calculated for corner gussets should be reevaluated in the case of middle gusset plates. Until a more detailed study is performed to evaluate the interface stresses, the authors recommend providing an interface weld that develops the shear strength of the gusset plate.

IN MEMORY OF PATRICK FORTNEY

The impact of losing Dr. Patrick Fortney during the course of this research is beyond words. Kind, knowledgeable, dedicated, and thoughtful are the words that are being echoed by his friends and colleagues when remembering and describing him. His knowledge in structural engineering—next to his experience in steel structure design, construction, and fabrication—made him the pioneering engineer to identify the chevron effect in the behavior of chevron beams in concentrically braced frames. Although his loss has left a great void in the steel industry, as well as his friends' and colleagues' hearts, his scientific findings and unique professional contributions will be remembered vividly forever.

SYMBOLS

A_g	Gross cross-section area of beam, in.^{2}
$A_{b\text{-}b}$	Normal (axial) force to section b-b limit state
C	Compression along the brace line limit state
Eql	Equal tension and compression brace loads on the assembly
F_{cr}	Critical stress, ksi
F_u	Specified minimum tensile strength, ksi
F_y	Specified minimum yield stress, ksi
H_1	Horizontal component of force in brace 1, kips
H_2	Horizontal component of force in brace 2, kips
L_1	Horizontal distance from the left edge of the gusset to the work point, in.
L_2	Horizontal distance from the right edge of the gusset to the work point, in.
L_g	Contact length of the gusset to beam interface, in.
M	Beam bending moment limit state
$M_{a\text{-}a}$	Moment acting at the gusset to beam interface, kip-in.
M_{max}	Beam maximum bending moment, kip-in.
Mec	Mechanism (buckling) loading on the assembly
$P_{compression}$	Brace compression strength, kips
$P_{post\text{-}buckling}$	Post-buckling strength, kips

$P_{tension}$	Brace tensile strength, kips
Pst	Post-buckling loading on the assembly
T	Tension along the brace line limit state
R_y	Ratio of the expected yield stress to the specified minimum yield stress
V	Beam shear force limit state
V_1	Vertical component of force in brace 1, kips
V_2	Vertical component of force in brace 2, kips
V_{max}	Maximum beam shear force, kips
Vb	V-bracing configuration
Xb	X-bracing configuration
a	Distance from left beam support to location of work point, in.
b	Distance from work point to right beam support, in.
e_b	Perpendicular distance from the gusset interface to the gravity axis of the frame beam, in.
h	Vertical distance of the gusset, in.
t_{gusset}	Gusset plate thickness
w_1	Net uniformly distributed transverse load on left half of gusset, kip/in.
w_2	Net uniformly distributed transverse load on right half of gusset, kip/in.
w.p.	Brace work point
Δ	Horizontal misalignment between the work point and the centroid of the gusset-to-beam interface, in.
ΣV_T	Summation of vertical components of brace forces, kips

REFERENCES

AISC (2016), *Seismic Provisions for Structural Steel Buildings*, ANSI/AISC 341-16, American Institute of Steel Construction, Chicago, Ill.

AISC (2017), *Steel Construction Manual*, American Institute of Steel Construction, Chicago, Ill.

ASCE (1998), *Handbook for the Seismic Evaluation of Buildings—A Prestandard*, FEMA-310, American Society of Civil Engineers, Washington, D.C.

Astaneh-Asl, A.,Goel, S.C., and Hanson, R.D. (1985), "Cyclic Out-of-Plane Buckling of Double-Angle Bracing," *Journal of Structural Engineering*, Vol. 111, No. 5, pp. 1,135–1,153.

Azad, S.K., Topkaya, C., and Astaneh-Asl, A. (2017), "Seismic Behavior of Concentrically Braced Frames Designed to Aisc341 and Ec8 Provisions," *Journal of Constructional Steel Research*, Vol. 133, pp. 383–404.

Bertero, V.V., Uang, C.-M., Llopiz, C.R., and Igarashi, K. (1989), "Earthquake Simulator Testing of Concentric Braced Dual System," *Journal of Structural Engineering*, Vol. 115, No. 8, pp. 1,877–1,894.

Bjorhovde, R. and Chakrabarti, S. (1985), "Tests of Full-Size Gusset Plate Connections," *Journal of Structural Engineering*, Vol. 111, No. 3, pp. 667–684.

Costanzo, S., D'Aniello, M., and Landolfo, R. (2017), "Seismic Design Criteria for Chevron Cbfs: European Vs North American Codes (Part-1)," *Journal of Constructional Steel Research*, Vol. 135, pp. 83–96.

D'Aniello, M., Costanzo, S., and Landolfo, R. (2015), "The Influence of Beam Stiffness on Seismic Response of Chevron Concentric Bracings," *Journal of Constructional Steel Research*, Vol. 112, pp. 305–324.

Fortney, P.J. and Thornton, W.A. (2015), "The Chevron Effect—Not an Isolated Problem," *Engineering Journal*, AISC, Vol. 52, No. 2, pp. 125–164.

Fortney, P.J. and Thornton, W.A. (2017), "The Chevron Effect and Analysis of Chevron Beams—A Paradigm Shift," *Engineering Journal*, AISC, Vol. 54, No. 4, pp. 263–296.

Hewitt, C.M. and Thornton, W.A. (2004), "Rationale Behind and Proper Application of the Ductility Factor for Bracing Connections Subjected to Shear and Transverse Loading," *Engineering Journal*, AISC, Vol. 41, No. 1, pp. 3–6.

Hsiao, P.C., Lehman, D.E., and Roeder, C.W. (2013), "A Model to Simulate Special Concentrically Braced Frames beyond Brace Fracture," *Earthquake Engineering & Structural Dynamics*, Vol. 42, No. 2, pp. 183–200.

Khatib, I.F., Mahin, S.A., and Pister, K.S. (1988), *Seismic Behavior of Concentrically Braced Steel Frames*, Earthquake Engineering Research Center, University of California.

Lee, S.-J. and Lu, L.-W. (1989), "Quasi-Static Tests of Scaled Model Building," *Journal of Structural Engineering*, Vol. 115, No. 8, pp. 1,895–1,916.

Lumpkin, E.J., Hsiao, P.-C., Roeder, C.W., Lehman, D.E., Tsai, C.-Y., Wu, A.-C., Wei, C.-Y., and Tsai, K.-C. (2012), "Investigation of the Seismic Response of Three-Story Special Concentrically Braced Frames," *Journal of Constructional Steel Research*, Vol. 77, pp. 131–144.

Naeim, F. (1998), "Performance of 20 Extensively-Instrumented Buildings during the 1994 Northridge Earthquake," *The Structural Design of Tall Buildings*, Vol. 7, No. 3, pp. 179–194.

Nascimbene, R., Rassati, G., and Wijesundara, K. (2012), "Numerical Simulation of Gusset Plate Connections with Rectangular Hollow Section Shape Brace under Quasi-Static Cyclic Loading," *Journal of Constructional Steel Research*, Vol. 70, pp. 177–189.

Okazaki, T., Lignos, D.G., Hikino, T., and Kajiwara, K. (2012), "Dynamic Response of a Chevron Concentrically Braced Frame," *Journal of Structural Engineering*, Vol. 139, No. 4, pp. 515–525.

Osteraas, J. and Krawinkler, H. (1989), "The Mexico Earthquake of September 19, 1985—Behavior of Steel Buildings," *Earthquake Spectra*, Vol. 5, No. 1, pp. 51–88.

Rega, G. and Vestroni, F. (1984), "Statistical Analysis of the Inelastic Response of Shear Structures Subjected to Earthquakes," *Earthquake Engineering & Structural Dynamics*, Vol. 12, No. 6, pp. 833–846.

Richard, R.M. (1986), *Analysis of Large Bracing Connection Designs for Heavy Construction*, AISC National Steel Construction Conference Proceedings.

Roeder, C.W., Lumpkin, E.J., and Lehman, D.E. (2011), "A Balanced Design Procedure for Special Concentrically Braced Frame Connections," *Journal of Constructional Steel Research*, Vol. 67, No. 11, pp. 1,760–1,772.

Roeder, C.W. and Popov, E.P. (1978), "Eccentrically Braced Steel Frames for Earthquakes," *Journal of the Structural Division*, Vol. 104, No. 3, pp. 391–412.

Sabelli, R., Mahin, S., and Chang, C. (2003), "Seismic Demands on Steel Braced Frame Buildings with Buckling-Restrained Braces," *Engineering Structures*, Vol. 25, No. 5, pp. 655–666.

Salawdeh, S., English, J., Goggins, J., Elghazouli, A.Y., Hunt, A., and Broderick, B.M. (2017), "Shake Table Assessment of Gusset Plate Connection Behaviour in Concentrically Braced Frames," *Journal of Constructional Steel Research*, Vol. 138, pp. 432–448.

Sen, A.D., Roeder, C.W., Berman, J.W., Lehman, D.E., Li, C.-H., Wu, A.-C., and Tsai, K.-C. (2016), "Experimental Investigation of Chevron Concentrically Braced Frames with Yielding Beams," *Journal of Structural Engineering*, Vol. 142, No. 12, pp. 04016123.

Shaw, S., Kanvinde, A., and Fell, B. (2010), "Earthquake-Induced Net Section Fracture in Brace Connections—Experiments and Simulations," *Journal of Constructional Steel Research*, Vol. 66, No. 12, pp. 1,492–1,501.

Shen, J., Wen, R., and Akbas, B. (2015), "Mechanisms in Two-Story X-Braced Frames," *Journal of Constructional Steel Research*, Vol. 106, pp. 258–277.

Simulia, D. (2013), "Abaqus 6.13 User's Manual," Dassault Systems, Providence, R.I.

Sloat, D. (2014), *Evaluation and Retrofit of Non-Capacity Designed Braced Frames*, Doctoral Dissertation, University of Washington.

Thornton, W. (1991), "On the Analysis and Design of Bracing Connections," *Proceedings of the AISC National Steel Construction Conference*.

Thornton, W.A. (1984), "Bracing Connections for Heavy Construction," *Engineering Journal*, Vol. 21, No. 3, pp. 139–148.

Tremblay, R. (2002), "Inelastic Seismic Response of Steel Bracing Members," *Journal of Constructional Steel Research*, Vol. 58, No. 5, pp. 665–701.

Tremblay, R. (2008), "Influence of Brace Slenderness on the Fracture Life of Rectangular Tubular Steel Bracing Members Subjected to Seismic Inelastic Loading," SEI Structures Congress.

Tremblay, R., Archambault, M.-H., and Filiatrault, A. (2003), "Seismic Response of Concentrically Braced Steel Frames Made with Rectangular Hollow Bracing Members," *Journal of Structural Engineering*, Vol. 129, No. 12, pp. 1,626–1,636.

Wallace, B.J. and Krawinkler, H. (1989), "Small-Scale Model Tests of Structural Steel Assemblies," *Journal of Structural Engineering*, Vol. 115, No. 8, pp. 1,999–2,015.

Wigle, V.R. and Fahnestock, L.A. (2010), "Buckling-Restrained Braced Frame Connection Performance," *Journal of Constructional Steel Research*, Vol. 66, No. 1, pp. 65–74.

Willibald, S., Packer, J., and Martinez-Saucedo, G. (2006), "Behaviour of Gusset Plate Connections to Ends of Round and Elliptical Hollow Structural Section Members," *Canadian Journal of Civil Engineering*, Vol. 33, No. 4, pp. 373–383.

Zhang, W., Huang, M., Zhang, Y.., and Sun, Y. (2011), "Cyclic Behavior Studies on I-Section Inverted V-Braces and Their Gusset Plate Connections," *Journal of Constructional Steel Research*, Vol. 67, No. 3, pp. 407–420.

The Indirect Analysis Method of Design for Stability: An Amplifier to Address Member Inelasticity, Member Imperfections, and Uncertainty in Member Stiffness

RAFAEL SABELLI

ABSTRACT

Design for stability requires multiple considerations, including geometric second-order effects (P-Δ and P-δ effects) and the effects on structure response of member inelasticity, member imperfections, and uncertainty in member stiffness. The "indirect analysis method" provides a simple amplifier approach to addressing these effects such that effective length factors may be taken as 1.0. The indirect analysis method meets the stability design requirements of the AISC *Specification* and can reduce analysis and design effort for many typical building structures.

Keywords: stability, direct analysis method, effective length, first-order analysis.

The indirect analysis method (IAM) provides a simple amplifier approach to addressing the effects on structure response of member inelasticity (including the effects of residual stress), member imperfections, and uncertainty in member stiffness. [Together the effects of these three factors (inelasticity, member imperfection, and stiffness uncertainty) are referred to here as *stiffness-reduction effects*.] The IAM permits second-order analysis with full stiffness properties; stiffness-reduction effects are addressed by an amplifier (B_3) applied to lateral loads prior to analysis or to their effects afterward. Verification studies confirm design forces consistent with the AISC *Specification* direct analysis method over a broad range of multiple parameters. The indirect analysis method can also be used as the basis of an improved first-order analysis method.

CURRENT METHODS OF DESIGN FOR STABILITY IN THE AISC *SPECIFICATION*

The AISC *Specification for Structural Steel Buildings*, hereafter referred to as the AISC *Specification*, defines three methods of design for stability (AISC, 2016): the direct analysis method (the DM, presented in Chapter C), the effective-length method (the ELM, presented in Appendix 7, Section 7.2), and the first-order analysis method (the FOM, presented in Appendix 7, Section 7.3). Each method includes coordinated analysis and design requirements that result in structures with sufficient strength to prevent instability, considering the structures' stiffness with respect to lateral displacement in the presence of vertical loads. Each method addresses stiffness-reduction effects differently, and each method requires either a second-order analysis (DM and ELM) or determination of the second-order effect (FOM). Second-order analysis may be either explicit or approximate, such as by means of the B_1 and B_2 factors [where B_1 and B_2 are the second-order effect multipliers for P-Δ and P-δ effects, respectively, defined in AISC *Specification* Appendix 8 (AISC, 2016)].

The DM addresses stiffness-reduction effects in the analysis, requiring a second-order analysis using reduced member stiffness. This produces the internal member forces that are expected to result from the application of the external forces, considering stiffness-reduction effects on the response of the structure. Stiffness-reduction effects in the DM are addressed both globally and member by member. Globally, all stiffness terms are reduced using a factor of 0.8. Additionally, the member flexural stiffness reduction for moment frame columns includes a term, τ_b, that relates to the member axial force, and thus at least one analysis iteration is required to determine the axial force corresponding to the loading condition. (Each load combination could entail its own particular set of member stiffness reductions, although grouping is typically done to reduce design effort.) Nevertheless, because the reduced stiffness of the DM model is not intended to be used for calculating drifts, a minimum of two models is typically required for building design: one for strength verification and another for drift determination [and period determination for seismic loads (ASCE, 2016)]. (Drift may be a service limit state, as is often the case for wind, or a safety limit state, as is the

Rafael Sabelli, Director of Seismic Design, Walter P Moore, San Francisco, Calif. Email: rsabelli@walterpmoore.com

Paper No. 2019-03R

case for seismic; in either case, full stiffness properties are used, although for different reasons.) With the DM, stability is adequately addressed without the need for an effective length factor, K, greater than 1.0. The DM defines notional lateral loads to represent initial system imperfections due to out-of-plumbness. These notional loads are required for gravity-only load combinations; they are also required for combinations that include other lateral loads for which the ratio of second-order drift to first-order drift exceeds 1.7 in the reduced-stiffness DM analysis.

The ELM addresses stiffness-reduction effects by requiring reduced compression strength (implemented by effective length factors in the design of columns) and addresses P-Δ effects by requiring a second-order analysis. The flexural demands imposed by columns that are near their stability limit on the column connections and on beams are not directly addressed in the ELM. This method allows for effective length factors to be taken as 1.0 for braced-frame columns and for moment-frame columns when $B_2 \leq 1.1$; determination of effective length factors for moment-frame columns is required when $B_2 > 1.1$. Several methods exist to account for the effect of leaning columns in determining effective length factors, with minor variation in the results (Geschwindner, 2002). The ELM is limited to cases in which the second-order effect does not exceed 1.5; gravity-only load combinations require notional loads. (The limit of 1.5 for a full-stiffness ELM model is equivalent to 1.7 for a reduced-stiffness DM analysis.)

In the FOM, stiffness-reduction and P-Δ effects are addressed together in the analysis by means of an additional lateral force in a first-order analysis. This force is derived in AISC Design Guide 28, Appendix B: "Development of the First-Order Analysis Method" (Griffis and White, 2013). To permit this simplification, limits are placed on both axial force in moment-frame columns and on second-order effects. FOM additional forces assume that second-order effects are at the maximum level permitted: $B_2 = 1.5$. Similar to the DM, the FOM allows for effective length factors to be taken as 1.0. Application of the additional lateral forces in the FOM for strength design does not guarantee that second-order effects on drift have been adequately addressed when consideration of these is required, such as by ASCE/SEI 7, Section 12.8.7 (ASCE, 2016), unless these forces are included in the drift analysis. Inclusion of such forces in the drift analysis is problematic for two reasons: Drift is typically checked in a separate analysis not subject to the same minima as the analysis for strength design; only geometric second-order effects, not stiffness-reduction effects, are required in drift determination (ASCE, 2016). While the FOM does not require a second-order analysis, its use requires that the second-order effect not exceed 1.5. Confirmation of this requires either a second-order analysis or calculation of the B_2 factor, and thus only modest additional effort would be required to incorporate second-order effects into the analysis.

THE INDIRECT ANALYSIS METHOD

The IAM is a simplified version of the DM, with stiffness-reduction effects addressed either globally or story by story rather than member by member. The IAM requires only relatively easy-to-implement means (second-order analysis and an amplification factor applied to lateral loads or to their effects) and does not require more cumbersome methods (such as determination of effective length factors greater than 1.0 or multiple models). The IAM incorporates both second-order analysis (either explicit second-order analysis or first-order analysis amplified by B_1 and B_2 factors) and an amplification factor to address stiffness reduction (B_3). This amplification factor is derived to amplify the second-order analysis forces such that the results obtained match those from the DM. Thus, the B_3 factor effectively performs the same function as the $0.8\tau_b$ stiffness reduction in the DM, permitting the use of effective length factors, K, of 1.0 in the IAM. Use of a global or story value of τ_b may make the IAM more conservative than the DM for cases with a wide range of moment-frame column axial force ratios.

General Stability Design Requirements

The AISC *Specification* requires five considerations for any admissible stability design method. These are listed in the following, along with the description of how each is addressed in the IAM. The approach to each consideration closely matches that for the DM, with the difference that items 3–5 utilize the B_3 factor, which incorporates $0.8\tau_b$, to address stiffness-reduction effects.

1. *Consider all deformations.* This requirement is addressed by proper modeling.
2. *Consider second-order effects (including P-Δ and P-δ effects).* This requirement is addressed by performing a second-order analysis, either explicit or through application of B_1 and B_2 factors.
3. *Consider geometric imperfections.* This requirement is addressed by application of notional loads (for the effect of structural imperfections on the structural response), application of the B_3 factor (for the effect of member imperfections on the structural response), and application of member strength formulae with $L_c = L$ (for the effect of member imperfections on member strength).
4. *Consider stiffness reduction due to inelasticity.* This requirement is addressed by application of the B_3 factor (for the effect on the structural response) and application of member strength formulae with $L_c = L$ (for the effect on member strength).

5. *Consider uncertainty in strength and stiffness.* This requirement is addressed by application of the B_3 factor (for the effect on the structural response) and application of member available strength formulae with $L_c = L$ (for the effect on member strength).

General Design Guidance

Although the investigation of stability effects tends to address systems near instability, examination of such cases should not be taken as endorsement of designing systems near instability. The limits proposed for the IAM are based solely on the verification of the method. As systems approach those limits, they become increasingly sensitive to the accuracy of loading assumptions, modeling, and analysis. Many engineers—including the author—apply lower limits on second-order and stiffness-reduction effects to their designs. Furthermore, it should be noted that for seismic design, ASCE/SEI 7, Section 12.8.7, limits the stability coefficient, θ, to 0.25 (or lower, for many systems). According to the ASCE/SEI 7 commentary (ASCE, 2016), the stability coefficient (using symbols from the AISC *Specification*) can be expressed as:

$$\theta = \frac{\alpha P_{story} \Delta_H}{HL} \tag{1}$$

where

H = total story shear, kips
L = story height, in.
P_{story} = total vertical load supported by the story, kips
α = ASD/LRFD force level adjustment factor, equal to 1.0 (LRFD) or 1.6 (ASD)
Δ_H = first-order interstory drift due to lateral forces, in.

Thus a limit on the stability coefficient, θ, is a limit on geometric stability (P-Δ) effects.

DERIVATION OF THE INDIRECT ANALYSIS METHOD

The IAM is derived from the DM, with the simplification that stiffness reductions, rather than being applied member by member, are computed story by story and applied either story by story or globally. This approach permits quantifying the effect and applying it as a factor in an analysis using full stiffness properties rather than requiring a modified model for stability design.

Following the method presented in Design Guide 28 (Griffis and White, 2013), the IAM is derived in the following based on a dual-purpose second-order amplifier, $\overline{B}_2$, that addresses both geometric nonlinearity (P-Δ effects) and the effects of stiffness reduction. [The $\overline{B}_2$ amplifier was developed as $\overline{B}_{lt}$ in White et al. (2007)]. Note that use of this amplifier to determine displacements is equivalent to establishing a reduced stiffness due to geometric effects combined with the effects of inelasticity, member imperfection, and stiffness uncertainty. The amplification has a nonlinear relationship to the destabilizing gravity load. However, the resulting stiffness defines a linear relationship between lateral load and displacement.

The second-order shear (with notional loads) is set equal to first-order shear with additional forces required for design for stability:

$$\overline{B}_2 (H + \sum N) = H + \overline{H}_{P\Delta} \tag{2}$$

where

$\overline{B}_2$ = second-order amplifier using the stiffness reduction $EI^* = 0.8\tau_b EI$
$\overline{H}_{P\Delta}$ = P-Δ shear forces [from Equation B-10b in Griffis and White (2013)], kips
ΣN = notional loads to address out-of-plumbness (at or above the level under consideration), kips

and

E = modulus of elasticity, ksi
I = moment of inertia, in.^{4}
τ_b = stiffness-reduction parameter defined in AISC *Specification* Section C2, Equations C2-2a and C2-2b

The AISC *Specification* definition of τ_b can be expressed as:

$$\tau_b = 4\frac{\alpha P_r}{P_{ns}}\left(1 - \frac{\alpha P_r}{P_{ns}}\right) \le 1.0 \tag{3}$$

where

P_{ns} = cross-section compressive strength, kips
= $F_y A_g$ (for columns without slender elements), kips
= $F_y A_e$ (for columns with slender elements), kips
P_r = required axial compressive strength using LRFD or ASD load combinations, kips

and

A_e = effective area, in.^{2}
A_g = gross area of member, in.^{2}
F_y = specified minimum yield stress, ksi

Griffis and White (2013) use an equality similar to Equation 2 to establish that FOM forces correspond to DM forces within the limits of FOM application. The displacement-magnification term $\overline{B}_2$ in the Design Guide 28 formulation [Equation B-4 in Griffis and White (2013)] incorporates a stiffness-reduction factor of 0.8 for the FOM:

$$\overline{B}_2 = \frac{1}{1 - Q/0.8} \tag{4}$$

where Q is a stability index, related to the stability coefficient θ; thus:

$$Q = \theta / R_M \tag{5}$$

and R_M is a coefficient to account for member P-δ influence on structure P-Δ.

The factor of 0.8 in Equation 4 represents the stiffness reduction of the DM, with the limitation that in the FOM, axial stress may not be permitted to reach a level sufficient to affect flexural stiffness of moment-frame beams and columns. A more general form of Equation 4 can be written to incorporate the axial-force-dependent flexural-stiffness-reduction parameter, τ_b:

$$\overline{B}_2 = \frac{1}{1 - Q / 0.8\tau_b} = \frac{1}{1 - \theta / 0.8\tau_b R_M} \tag{6}$$

Incorporation of τ_b into $\overline{B}_2$ effectively applies this parameter uniformly to all members and all actions (axial as well as flexure). This extensive application of τ_b to the entire lateral load effect potentially overestimates its influence but permits the derivation of a single factor on the lateral load to account for the effect of high axial stress on the system stiffness.

The stability index, Q, can also be expressed thus:

$$Q = \frac{\alpha P_{story} \Delta_H}{R_M HL} \tag{7}$$

The stability index Q is thus more complete than the stability coefficient θ, including the stiffness reduction related to moment-frame column compressive force, R_M. The stability coefficient, θ, however, is used in the ASCE 7 standard (ASCE, 2016) and is therefore used in this paper (in conjunction with R_M). The terms that define the stability index Q in Equation 7 can also be used to define the B_2 amplifier:

$$B_2 = \frac{1}{1 - \dfrac{\alpha P_{story} \Delta_H}{R_M HL}} \tag{8}$$

Thus, the index Q can be expressed as a function of B_2:

$$Q = 1 - \frac{1}{B_2} \tag{9}$$

For development of the IAM, the geometric effects and stiffness-reduction effects that comprise the factor $\overline{B}_2$ are distinguished:

$$\overline{B}_2 = B_2 B_3 \tag{10}$$

where

B_3 = IAM amplification factor to account for stiffness reduction due to inelasticity, member imperfection, and stiffness uncertainty

Thus, B_2 addresses geometric second-order effects, and B_3 addresses stiffness reduction due to inelasticity, member imperfection, and stiffness uncertainty. This separation permits the use of typical second-order analysis using nominal stiffness properties with a separate factor, B_3, to account for the effects of the stiffness reduction inherent in the DM. By separating B_2 and B_3, the IAM does not affect established second-order analysis procedures that use full-stiffness member properties, including those incorporated into analysis software. [Use of the B_2 amplifier is valid only for systems with vertical columns (AISC, 2016), and thus the IAM (which utilizes B_2) is similarly limited.]

Combining Equation 6 and Equation 10 gives:

$$B_2 B_3 = \frac{1}{1 - \theta / 0.8\tau_b R_M} \tag{11}$$

The second-order amplifier B_2 can also be written in similar terms (similar to Equation B-3 in Griffis and White, 2013):

$$B_2 = \frac{1}{1 - \theta / R_M} \tag{12}$$

Equation 11 and Equation 12 are combined to determine B_3:

$$B_3 = \frac{1 - \theta / R_M}{1 - \theta / 0.8\tau_b R_M} \tag{13}$$

The factor B_3 is a function of the stability coefficient, θ, the P-δ factor, R_M, and the flexural-stiffness-reduction parameter, τ_b. Limits on these values can be set in advance of design such that the factor B_3 may be determined and incorporated into the analysis from the first iteration. (B_3 is also fundamentally an expression of the 0.8 stiffness-modifier term, but this parameter is fixed.)

Equation 13 can be written in terms of B_2 and τ_b utilizing Equation 9 and Equation 5:

$$B_3 = \frac{0.8\tau_b}{1 - (1 - 0.8\tau_b) B_2} \tag{14}$$

Equation 13 or 14 may be used to amplify the results of a second-order analysis. If $\alpha P_r / P_{ns} \le 0.5$, $\tau_b = 1.0$, and Equation 14 reduces to:

$$B_3 = \frac{4}{5 - B_2} \tag{15}$$

USE OF THE SECOND-ORDER EFFECT DETERMINED FROM ANALYSIS

If an explicit second-order analysis is performed, a second-order amplification term may be determined from the analysis results and used in lieu of B_2 from AISC *Specification* Equation A8-6 to calculate the stiffness-reduction amplifier.

This amplification term (shown here as B_2') is determined using the ratio of second-order displacements to first-order displacements from the analysis:

$$B_2' = \frac{\Delta_2}{\Delta_1} \tag{16}$$

where

Δ_1 = first-order story drift using full stiffness properties, in.

Δ_2 = second-order story drift using full stiffness properties, in.

The corresponding stiffness-reduction amplifier, B_3', is obtained by combining Equation 14 and Equation 16 (with $B_2 = B_2'$):

$$B_3' = \frac{0.8\tau_b}{1-[1-0.8\tau_b]^{\Delta_2/\Delta_1}} \tag{17}$$

Notional Loads

The IAM notional loads are the same as are required for the DM. These notional loads are:

$$N_i = \frac{\Delta_o}{L} Y_i \tag{18}$$

where

N_i = notional load at level i, kips

Y_i = gravity load applied at level i, kips

Δ_o = nominal initial out-of-plumbness, in.

The initial out-of-plumbness, Δ_o, is taken as 0.002 times the story height in the AISC *Specification* (AISC, 2016). Notional loads are applied story by story, and thus accumulate as the vertical load supported, P_{story}, accumulates.

Consistent with the DM, these notional loads are proposed to be applied for gravity-only load combinations for cases with $B_2 \le 1.5$ and for all load combinations with $B_2 > 1.5$. This results in a minor error for load combinations that include lateral loads and have $B_2 \le 1.5$; this too is consistent with the DM.

As the IAM has been derived to be consistent with the DM, the alternative of using an additional notional load equal to 0.001 times the gravity load and $\tau_b = 1.0$ in lieu of $\tau_b < 1.0$ may be used [AISC *Specification*, C2.3(c)].

Values of B_3 and Proposed Range of Applicability of the Indirect Analysis Method

Table 1 shows the factor B_3 for different combinations of B_2 and the flexural stiffness-reduction parameter, τ_b, using Equation 14. Values of B_3 are presented corresponding to the values of B_2 ranging from 1.00 to 5.00 and $\alpha P_r/P_{ns}$ ranging from 0 to 1.00. $B_2 = 1.0$ corresponds to a system that has no gravity load (or is infinitely stiff). $B_2 = 5.00$ and $\alpha P_r/P_{ns} = 1.00$ conditions are unstable regardless of other factors. Shading indicates bands of similar values. Linear interpolation may be used with this table to obtain a liberal estimate of B_3.

The B_3 amplifier increases disproportionately with increasing axial-load ratios $\alpha P_r/P_{ns}$ and second-order amplifier B_2. At higher ranges of these parameters, the calculation results in negative or zero values, indicating insufficient stiffness to prevent instability regardless of strength; these cases are shown in black. High values of B_3 indicate high sensitivity to loading and modeling assumptions. In practice, a limit on the permissible B_3 value may be used to prevent large sensitivity to small approximations, errors, or uncertainties in loading or modeling.

The IAM is not proposed for $B_2 > 2.0$ due to this sensitivity. For $B_2 > 1.5$, a second-order analysis that includes the effect of P-δ on P-Δ is necessary (Nair, 2009). (While use of a B_2 amplifier that includes R_M complies with this requirement, an explicit second-order analysis reduces error.) Similarly, the IAM is not proposed for $\alpha P_r/P_{ns} > 0.7$ for moment-frame columns.

The proposed IAM may be used if the following conditions are met:

- $\alpha P_r/P_{ns} \le 0.7$ for moment-frame columns.
- Columns are vertical.
- A second-order analysis is performed (or the factors B_1 and B_2 are applied).
- Notional loads are applied for $B_2 > 1.5$ and for gravity-only load combinations.
- B_3 is taken as the largest value at or above the level under consideration.
- The value of τ_b is determined (or confirmed) using the results of a second-order analysis that is amplified using the factor B_3.
- The largest displacement of the story is used to determine both B_2 and B_3.

For torsional loading (i.e., lateral loading that causes the diaphragm to rotate), Equations 16 and 17 may be used with results from a three-dimensional analysis, or values of B_2 and B_3 may be computed based on maximum drifts. Notional load patterns should include a torsion-inducing pattern.

FIRST-ORDER ANALYSIS

Engineers accustomed to performing a first-order analysis may prefer to use amplifiers to address both second-order effects (B_2) and the stiffness-reduction (B_3). This product,

obtained by multiplying Equation 14 by B_2, may be applied to the lateral loads or to their effects determined using a first-order analysis:

$$B_2B_3 = \frac{0.8\tau_b}{1/B_2 - (1-0.8\tau_b)} \quad (19)$$

This product is also a useful indication of the magnitude of stability effects on the design. Such an approach is a version of the IAM (rather than the FOM), and the limits discussed in the previous section apply. If $\alpha P_r/P_{ns} \le 0.5$, $\tau_b = 1.0$, and Equation 19 reduces to:

$$B_2B_3 = \frac{4}{5/B_2 - 1} \quad (20)$$

This equation can be used as an amplification factor on lateral loads with greater economy compared to the FOM, with results corresponding to those that would be obtained from the DM. At $B_2 = 1.5$ this equation results in $B_2B_3 = 1.71$, and for gravity-only load combinations, the amplified notional load (B_2B_3N) is $1.71 \times 0.002P_{story} = 0.00343P_{story}$, 82% of what is required by the FOM in the AISC *Specification*. [This difference is due to the conservative amplification of the initial out-of-plumbness, Δ_o, in the FOM by dividing by 0.8, which simplifies the FOM derivation (Equation B-9b in Griffis and White, 2013).] The advantage provided by the IAM is greater at lower values of B_2 because the FOM forces are based on $B_2 = 1.5$ regardless of the actual second-order effect.

Table 2 shows the product of the factors B_2 and B_3 for different combinations of B_2 and flexural stiffness-reduction parameter, τ_b. The table utilizes Equation 19 (B_2B_3). Similar to Table 1, shading in Table 2 marks bands of similar values. Linear interpolation may be used with this table to obtain a liberal estimate of the product B_2B_3.

APPLICATION

Similar to the DM, the IAM addresses the stiffness-reduction effects in the analysis rather than in the design strength equations (as the ELM does). As discussed in the derivation, the B_2 and B_3 amplifiers represent a reduced linear lateral stiffness. The IAM amplification may thus be applied to loads prior to the second-order analysis or to their effects afterward, prior to design, or (conservatively) to demand-to-capacity ratios. Simpler methods of application are necessarily more conservative. Methods of application include:

- *Demand-to-capacity ratio limit.* The simplest method is to use the inverse of the factor B_3 as a limit on permissible demand-to-capacity ratios. This method effectively amplifies the gravity load effect, which introduces arbitrary conservatism; this may be acceptable for cases where B_3 is small. For example, in seismic design per ASCE/SEI 7 (ASCE, 2016), limits on the stability coefficient, θ, for special moment frames are such that if $\alpha P_r/P_{ns} \le 0.5$, the product B_2B_3 cannot exceed 1.15; for this value, demand-to-capacity ratios not exceeding 0.866 for a first-order analysis are acceptable without more refined amplification and combination of loads.
- *Amplification of loads.* Alternatively, the value of B_3 can be selected in advance of design by limiting $\alpha P_r/P_{ns}$ and taking B_2 as the lesser of that corresponding to the limit on the stability coefficient, θ, and that corresponding to the drift limit. This value of B_3 may be applied as a supplementary lateral load factor. The factor B_3 may be used to amplify the entire set of results from a lateral analysis, utilizing the largest value of B_3 for all stories. Because B_3 is based on the smallest value of τ_b for all moment-frame columns in a story, this may extend the effect of a single low value of τ_b dramatically, but in typical practice, moment-frame columns rarely have axial force above $0.5P_{ns}$, and the axial force must be substantially greater than this value to have a significant effect on stiffness. If some $\alpha P_r/P_{ns}$ ratios exceed 0.5 (and member selection is governed by strength rather than the stiffness required to meet drift limits), story-by-story application of B_3 may be preferable.
- *Story-by-story amplification of load effects.* Use of a single value of B_3 on the entire lateral load will be conservative for stories where the second-order effect is relatively low. B_3 may be applied to the load effect story by story instead of as a global factor. However, use of the B_3 factor as a story-specific factor on the applied force (rather than on the load effect) is potentially unconservative because the amplification of overturning effects is less than the shear amplification at levels with a higher value of B_3 than the levels above (which is typical if drifts are uniform), and thus this method is not recommended until this potential discrepancy is studied. Story-by-story application of the product B_2B_3 on the lateral load effect is straightforward with superposition of load effects from a first-order analysis. Story-by-story application of factor B_3 with the results of a second-order analysis may be done by developing a model with geometric stiffness based on the vertical loads; analyses using this geometric-stiffness model are suitable for linear superposition (Wilson and Habibullah, 1987) and are thus suitable for application of the B_3 factor either to lateral loads or lateral-load effects.

The proposed procedure for IAM application is:

1. Establish limit on drift and corresponding vertical and lateral loads.
2. Establish vertical and lateral loads for strength evaluations.

Table 1. Amplification Factors B_3 for IAM

$\alpha P_r/P_{ns}$	≤0.5	0.55	0.6	0.65	0.7	0.75	0.8	0.85	0.9	0.95	1.00
τ_b	1	0.99	0.96	0.91	0.84	0.75	0.64	0.51	0.36	0.19	0.00
B_2	B_3										
1.00	1.00	1.00	1.00	1.00	1.00	1.00	1.00	1.00	1.00	1.00	
1.05	1.01	1.01	1.02	1.02	1.03	1.03	1.05	1.08	1.14	1.39	
1.10	1.03	1.03	1.03	1.04	1.05	1.07	1.11	1.17	1.33	2.26	
1.15	1.04	1.04	1.05	1.06	1.08	1.11	1.17	1.28	1.59	6.13	
1.20	1.05	1.06	1.06	1.08	1.11	1.15	1.24	1.41	1.98		
1.25	1.07	1.07	1.08	1.10	1.14	1.20	1.31	1.57	2.62		
1.30	1.08	1.09	1.10	1.13	1.17	1.25	1.40	1.77	3.87		
1.35	1.10	1.10	1.12	1.15	1.21	1.30	1.50	2.03	7.42		
1.40	1.11	1.12	1.14	1.18	1.24	1.36	1.62	2.38	90.0		
1.45	1.13	1.13	1.16	1.20	1.28	1.43	1.75	2.88			
1.50	1.14	1.15	1.18	1.23	1.32	1.50	1.91	3.64			
1.55	1.16	1.17	1.20	1.26	1.37	1.58	2.10	4.95			
1.60	1.18	1.19	1.22	1.29	1.41	1.67	2.34	7.73			
1.65	1.19	1.21	1.24	1.32	1.46	1.76	2.63	17.6			
1.70	1.21	1.23	1.27	1.35	1.52	1.88	3.00				
1.75	1.23	1.25	1.29	1.39	1.58	2.00	3.51				
1.80	1.25	1.27	1.32	1.43	1.64	2.14	4.21				
1.85	1.27	1.29	1.35	1.47	1.71	2.31	5.27				
1.90	1.29	1.31	1.37	1.51	1.78	2.50	7.03				
1.95	1.31	1.33	1.40	1.55	1.86	2.73	10.6				
2.00	1.33	1.36	1.43	1.60	1.95	3.00	21.3				
2.20	1.43	1.46	1.57	1.81	2.41	5.00					
2.40	1.54	1.58	1.73	2.10	3.16	15.0					
2.60	1.67	1.72	1.94	2.49	4.57						
2.80	1.82	1.90	2.19	3.05	8.24						
3.00	2.00	2.11	2.53	3.96	42.0						
3.50	2.67	2.91	4.09	15.2							
4.00	4.00	4.71	10.7								
4.50	8.00	12.4									
5.00											

Unstable

3. Size members to meet drift limit.
4. Check stability coefficient limit θ, if required (as it is for seismic design).
5. Determine second-order effect B_2 (Equation 12) for the applicable load combinations.
6. Calculate preliminary value of B_3 (based on $\alpha P_r/P_{ns} \leq 0.5$ using Equation 15).
7. Apply additional notional load of $0.001P_{story}$ to preclude the need to check $\alpha P_r/P_{ns}$. (This is optional; engineers may consider the check on axial load ratio to be less cumbersome than implementing the notional load. Also, this notional-load approach may result in a more conservative evaluation.)
8. Perform second-order analysis with lateral loads amplified by the largest value of B_3.

Table 2. Amplification Factors B_2B_3 for IAM											
$\alpha P_r/P_{ns}$	≤0.5	0.55	0.6	0.65	0.7	0.75	0.8	0.85	0.9	0.95	1.00
τ_b	1	0.99	0.96	0.91	0.84	0.75	0.64	0.51	0.36	0.19	0.00
B_2	B_2B_3										
1.00	1.00	1.00	1.00	1.00	1.00	1.00	1.00	1.00	1.00	1.00	
1.05	1.06	1.06	1.07	1.07	1.08	1.09	1.10	1.13	1.20	1.46	
1.10	1.13	1.13	1.13	1.14	1.16	1.18	1.22	1.29	1.46	2.49	
1.15	1.19	1.20	1.20	1.22	1.24	1.28	1.34	1.47	1.83	7.05	
1.20	1.26	1.27	1.28	1.30	1.33	1.38	1.48	1.69	2.37		
1.25	1.33	1.34	1.35	1.38	1.42	1.50	1.64	1.96	3.27		
1.30	1.41	1.41	1.43	1.46	1.52	1.63	1.82	2.30	5.03		
1.35	1.48	1.49	1.51	1.55	1.63	1.76	2.03	2.74	10.0		
1.40	1.56	1.56	1.59	1.65	1.74	1.91	2.26	3.34	126		
1.45	1.63	1.64	1.68	1.74	1.86	2.07	2.54	4.18			
1.50	1.71	1.73	1.77	1.84	1.98	2.25	2.87	5.46			
1.55	1.80	1.81	1.86	1.95	2.12	2.45	3.26	7.67			
1.60	1.88	1.90	1.95	2.06	2.26	2.67	3.74	12.4			
1.65	1.97	1.99	2.05	2.18	2.42	2.91	4.34	29.0			
1.70	2.06	2.08	2.16	2.30	2.58	3.19	5.11				
1.75	2.15	2.18	2.26	2.43	2.76	3.50	6.14				
1.80	2.25	2.28	2.37	2.57	2.95	3.86	7.58				
1.85	2.35	2.38	2.49	2.71	3.16	4.27	9.74				
1.90	2.45	2.49	2.61	2.86	3.39	4.75	13.4				
1.95	2.56	2.60	2.73	3.02	3.64	5.32	20.6				
2.00	2.67	2.71	2.87	3.19	3.91	6.00	42.7				
2.20	3.14	3.21	3.45	3.99	5.31	11.0					
2.40	3.69	3.80	4.16	5.03	7.58	36.0					
2.60	4.33	4.48	5.03	6.46	11.9			Unstable			
2.80	5.09	5.31	6.14	8.55	23.1						
3.00	6.00	6.32	7.58	11.9	126						
3.50	9.33	10.2	14.3	53.1							
4.00	16.0	18.9	42.7								
4.50	36.0	55.7									
5.00											

9. Verify that member demand-to-capacity ratios do not exceed 1.0. If $\alpha P_r/P_{ns} \leq 0.5$ was assumed (see step 7), check this ratio.

10. If the strength or stability checks indicate insufficiency, iterate using IAM or switch to DM. For IAM iteration, check $\alpha P_r/P_{ns}$ (to determine if the additional notional load can be removed), recalculate B_3, consider applying separate B_3 factors at each story, or resize members.

Steps 4, 5, and 6 may be done in advance of design by assuming a stiffness necessary to meet drift limits (including second-order effects), simplifying the design process. (The design example in Appendix C follows this procedure.)

Because many moment frames have member sizes selected to meet drift limits rather than for strength, iteration in the subsequent design for stability is not always required, and the IAM provides a relatively simple method of verifying adequate strength to maintain stability. If iteration is required and the DM is used, the initial IAM analysis provides the necessary information to determine τ_b.

Table 3. Comparison of Methods of Design for Stability		
	Advantages of IAM	**Disadvantages of IAM**
FOM	• Lower forces. • Permits $\alpha P_r/P_{ns} \le 0.7$ instead of $\alpha P_r/P_{ns} \le 0.5$ for moment frame columns. • Permits $B_2 \le 2.0$ instead of $B_2 \le 1.5$. • Eliminates the need for additional lateral loads (for $B_2 \le 1.5$). • B_2B_3 is an indicator of the sensitivity to modeling and loading assumptions.	• Requires second-order analysis. However, the FOM is limited to $B_2 \le 1.5$ and thus requires determination of the second-order effect to permit use.
ELM	• Lower demand-to-capacity ratios. • $K = 1$ for moment-frame columns with $B_2 > 1.1$. • Permits $B_2 \le 2.0$ instead of $B_2 \le 1.5$. • Provides appropriate design forces for beams and connections (instead of addressing only column strength). • B_3 is an indicator of the sensitivity to modeling and loading assumptions.	• Requires application of amplification factor B_3. • Limited to $\alpha P_r/P_{ns} \le 0.7$ for moment frame columns.
DM	• Single calculation of B_3 per level in lieu of member-by-member application of τ_b. • Does not require one model for strength and a second model for drift and period determination. • B_3 is an indicator of the sensitivity to modeling and loading assumptions.	• Potentially higher forces, especially for torsional response and flexible diaphragms. • Requires use of largest τ_b for each level of moment frames if $\alpha P_r/P_{ns} > 0.5$. • Suitability limited to: ◦ Vertical columns. ◦ $B_2 \le 2.0$. ◦ $\alpha P_r/P_{ns} \le 0.7$ for moment frame columns.

For mixed systems (moment frames with braced frames or shearwalls), R_M determined using AISC *Specification* Equation A-8-8 is appropriate to use in calculating B_3. The axial-force ratio $\alpha P_r/P_{ns}$ is only relevant for members whose flexural resistance contributes to the lateral stiffness; braces, beams, and columns modeled with both ends pinned may have $\alpha P_r/P_{ns} > 0.5$ and not be considered in determining the value of τ_b to be used to compute B_3.

VERIFICATION

Verification studies are presented in Appendices A, B, and C. Appendix A applies the IAM to a simple frame that was studied by Carter and Geschwindner (2008) using FOM, ELM, and DM methods. That study demonstrated the advantage of the DM over the ELM and FOM in terms of lower demand-to-capacity ratios, and Appendix A shows a perfect correspondence between the IAM and the DM. Appendix B is a multi-parameter study of similar frames, comparing IAM and DM forces and design demand-to-capacity ratios. This comparison indicates an excellent correlation between design checks using DM and IAM forces over a broad range of the second-order effect (B_2), column slenderness, and stiffness-reduction parameter, τ_b. Appendix C is a design example of a two-bay, eight-story frame, demonstrating application of the method in the design process.

QUALITATIVE COMPARISON OF THE PROPOSED INDIRECT ANALYSIS METHOD WITH OTHER METHODS

Table 3 shows qualitative advantages and disadvantages of the proposed IAM with respect to the established stability design methods (DM, ELM, and FOM).

CONCLUSIONS

The proposed indirect analysis method (IAM) is a stability design method based on the DM and developed to reduce the effort required of the designer. Calculation of the factors utilized in the IAM (B_2 and B_3) may be performed in advance of design and can be used to identify cases in which a more rigorous method of analysis and design for stability is appropriate. IAM is proposed to be limited to $B_2 \le 2.0$ and $\alpha P_r/P_{ns} \le 0.7$. Above these limits, the structure is highly sensitive to second-order effects and stiffness reduction (and thus to the accuracy of loading assumptions, modeling, and analysis).

The IAM has been compared to the DM for a range of second-order effects and axial-force ratios. Comparisons indicate close correlation, with the IAM becoming less conservative for cases with high column slenderness and high P-Δ effects (B_2). Within the proposed range of applicability,

the IAM approximates the DM very closely, with differences in demand-to-capacity ratio no greater than 1%.

The IAM is particularly well suited for designs governed by drift or stability-coefficient limits (such as for seismic design), allowing a simple confirmation of compliance with AISC stability-design requirements with a single factor. Thus, drift design and strength design, which are two distinct analyses, often with different loadings, may be performed using a single model without changing member properties for steel structures. For strength-governed designs, the IAM entails a modest degree of conservatism, which can be reduced by a story-by-story application of factors on the lateral-load effect.

The IAM can be used as the basis for an improved FOM with less conservatism and a better indication of the magnitude of stability-related effects on the design.

The IAM matches the DM for structures that have moment-frame columns with an axial-load ratio of $\alpha P_r/P_{ns} \leq 0.5$; it is conservative compared to the DM for structures that have moment frame columns with differing levels of axial-load ratio $\alpha P_r/P_{ns}$ above 0.5. The level of conservatism of the IAM has not been established for more complex structures, although if member selection is governed by drift, the level of conservatism in the strength evaluation is inconsequential.

ACKNOWLEDGMENTS

Any reader of this paper will note its debt to the work of Griffis and White. Additionally, Larry Griffis provided valuable guidance in the development of this method. Matt Eatherton was a careful early reviewer who identified that this method is not limited to seismic applications. Lou Geschwindner provided a detailed review that helped clarify how this method differs from the other stability design methods. Ron Ziemian guided the use of more exact solutions incorporated into the verification study. Larry Kruth and Leigh Arber provided encouragement and helped focus this work on providing a benefit to practicing engineers. My colleagues Ozgur Atlayan, Joseph Dowd, and Susendar Muthukumar provided detailed review and assisted in the verification and application.

ABBREVIATIONS

ASD	Allowable strength design per AISC *Specification* Chapter B
DCR	Demand-to-capacity ratio
DM	Direct analysis method of design for stability per AISC *Specification* Chapter C
ELM	Effective-length method of design for stability per AISC *Specification* Appendix 7
IAM	Indirect analysis method of design for stability
FOM	First-order analysis method of design for stability per AISC *Specification* Appendix 7
LRFD	Load and resistance factor design per AISC *Specification* Chapter B

SYMBOLS

A_e	Effective area, in.^{2} (AISC *Specification*)
A_g	Gross area of member, in.^{2} (AISC *Specification*)
B_2	Multiplier to account for P-Δ effects (AISC *Specification* Appendix 8)
$\overline{B}_2$	Second-order amplifier using the stiffness reduction $EI^* = 0.8\tau_b EI$ (Design Guide 28)
B_2'	Second-order effect determined from second-order analysis results (Equation 16)
B_3	IAM amplification factor to account for stiffness reduction due to inelasticity, member imperfection, and stiffness uncertainty (Equation 14)
B_3'	IAM amplification factor to account for stiffness reduction due to inelasticity, member imperfection, and stiffness uncertainty calculated using B_2' (Equation 17)
C_L	Factor that accounts for the reduction in column sidesway stiffness due to the presence of axial load on the column (Design Guide 28)
D_{AF}	Displacement amplification factor (Design Guide 28)
$D_{AF\text{-}DM}$	Displacement amplification factor using reduced stiffness (Appendix B)
E	Modulus of elasticity, ksi (AISC *Specification*)
F_{AF}	Force amplification factor (Design Guide 28)
$F_{AF\text{-}DM}$	Force amplification factor using reduced stiffness (Appendix B)
F_y	Specified minimum yield stress, ksi (AISC *Specification*)
H	Total story shear, kips (AISC *Specification*)
$\overline{H}_{P\Delta}$	P-Δ shear forces, kips (Design Guide 28)
I	Moment of inertia, in.^{4} (AISC *Specification*)
K	Effective length factor (AISC *Specification* Chapter E)
L	Story height, in. (AISC *Specification*)

M_{DM} Moment resulting from a second-order analysis using reduced stiffness as required by the direct analysis method, kip-in. (Appendix B)

M_{FOA} First-order analysis moment, kip-in. (Appendix B)

M_{SOA} Second-order analysis moment, kip-in. (Appendix B)

N_i Notional load at level *i*, kips (AISC *Specification*)

ΣP Sum of applied vertical forces, kips, (Design Guide 28)

P Applied vertical force, kips, (Design Guide 28)

P_A Axial force in stability column, kips (Appendix B)

P_B Axial force in leaning column, kips (Appendix B)

P_L Story lateral force required to induce a first-order unit drift, kips (Design Guide 28)

P_{e1} Elastic critical buckling strength of the member in the plane of bending, kips (AISC *Specification*)

P_{ns} Cross-section compressive strength, kips (AISC *Specification*)

P_r Required axial compressive strength, kips (AISC *Specification*)

P_{story} Total vertical load supported by the story, kips (AISC *Specification*)

Q Stability index (Design Guide 28)

R_M Coefficient to account for member P-δ influence on structure P-Δ (AISC *Specification*)

Y_i Gravity load applied at level *i*, kips (AISC *Specification*)

α ASD/LRFD force level adjustment factor, equal to 1.0 (LRFD) or 1.6 (ASD) (AISC *Specification*)

α Ratio of the smaller to the larger end moment in the moment-frame column, determined from a first-order sidesway analysis (Design Guide 28)

β_L Coefficient corresponding to the contribution of the moment-frame column to the first-order story sidesway stiffness (Design Guide 28)

Δ_1 First-order story drift using full stiffness properties, in.

Δ_2 Second-order story drift using full stiffness properties, in.

Δ_{DM} Second-order story drift using reduced stiffness properties, in. (Appendix B)

Δ_H First-order interstory drift due to lateral forces, in. (AISC *Specification*)

Δ_o Nominal initial out-of-plumbness, in. (Design Guide 28)

θ Stability coefficient for P-Δ effects (ASCE/SEI 7)

τ_b Flexural stiffness-reduction parameter (AISC *Specification*)

REFERENCES

AISC (2005), *Specification for Structural Steel Buildings*, ANSI/AISC 360-05, American Institute of Steel Construction, Chicago, Ill.

AISC (2016), *Specification for Structural Steel Buildings*, ANSI/AISC 360-16, American Institute of Steel Construction, Chicago, Ill.

ASCE (2016), *Minimum Design Loads and Associated Criteria for Buildings and Other Structures*, ASCE/SEI 7-16, American Society of Civil Engineers, Reston, Va.

Carter, C.J. and Geschwindner, L.F. (2008), "A Comparison of Frame Stability Analysis Methods in ANSI/AISC 360-05," *Engineering Journal*, AISC, Vol. 45, No. 3, pp. 159–170.

Geschwindner, L.F. (2002), "A Practical Look at Frame Analysis, Stability and Leaning Columns," *Engineering Journal*, AISC, Vol. 39, No. 4, pp. 167–181.

Griffis, L.G. and White, D.W. (2013), *Stability Design of Steel Buildings,* Design Guide 28, AISC, Chicago, Ill.

LeMessurier, W.J. (1977), "A Practical Method of Second Order Analysis Part 2; Rigid Frames," *Engineering Journal*, AISC, Vol. 14, No. 2, pp. 49–67.

Nair, R.S. (2009), "A Model Specification for Stability Design by Direct Analysis," *Engineering Journal*, AISC, Vol. 46, No. 1, pp. 28–38.

Surovek-Maleck, A. and White, D.W. (2004), "Alternative Approaches for Elastic Analysis and Design of Steel Frames. I: Overview," *Journal of Structural Engineering*, ASCE, Vol. 130, No. 8, pp. 1,186–1,196.

White, D.W., Maleck, A.E., and Kim, S.-C. (2007), "Direct Analysis and Design Using Amplified First-Order Analysis, Part 1: Combined Braced and Gravity Framing Systems," *Engineering Journal*, AISC, Vol. 44, No. 4, pp. 305–322.

Wilson, E.L. and Habibullah, A. (1987), "Static and Dynamic Analysis of Multi-Story Buildings Including P-Delta Effects," *Earthquake Spectra*, EERI, Vol. 3, No. 2, pp. 289–298.

APPENDIX A

VERIFICATION: CANTILEVER STABILITY COLUMN WITH LEANING COLUMN (EXAMPLE)

The equivalence between the IAM and the DM can be established by analyzing a well-understood example frame: the one-bay frame studied by Carter and Geschwindner (2008). The frame consists of a cantilevered stability column (left, with a rigid base connection and a pin at the top), a leaning column (right, with pins top and bottom), and a rigid beam constraining their lateral movement. This frame is shown in Figure A1. The LRFD method is employed in this example.

Carter and Geschwindner used the following values for their study:

$P_A = P_B = 200$ kips

$L = 15$ ft

$H = 20$ kips

The notional load N depends on the stability-design method employed. (No notional load is required for the IAM in this example.) The stability column is an ASTM A992 W14×90.

Carter and Geschwindner determined axial forces and moments for four different methods of design for stability:

- The effective-length method (second order).
- The first-order method.
- The direct analysis method.
- The simplified method (a version of the ELM utilizing design tables).

The IAM is applied to this frame, utilizing the results of Carter and Geschwindner's full-stiffness second-order analysis for the system and for column A. The determination of B_2 is redone here to add a significant figure. (Such precision is not required for the IAM but is applied in this example to allow comparison of results without artifacts due to rounding.) Consistent with the 2005 edition of the AISC *Specification* (AISC, 2005), Carter and Geschwindner use a value of R_M of 0.85 rather than calculating R_m using AISC *Specification* Equation A-8-8 per the 2016 edition (AISC, 2016); for purposes of comparison of the stability-design methods, the same value is used here.

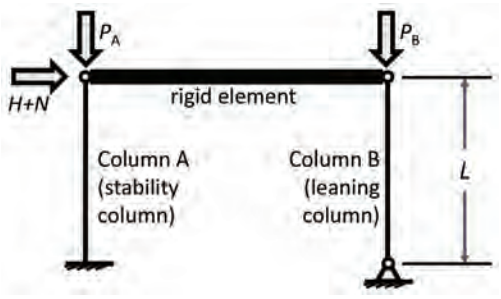

Fig. A1. Frame used for verification study.

$$\Delta_H = \frac{HL^3}{3EI}$$
$$= \frac{(20 \text{ kips})\left[(15 \text{ ft})(12 \text{ in./ft})\right]^3}{3(29{,}000 \text{ ksi})(999 \text{ in.}^4)}$$
$$= 1.34 \text{ in.}$$

$$B_2 = \frac{1}{1 - \frac{\alpha P_{story} \Delta_H}{R_M HL}} \quad (8)$$
$$= \frac{1}{1 - \frac{1.0(400 \text{ kips})(1.34 \text{ in.})}{0.85(20 \text{ kips})(180 \text{ in.})}}$$
$$= 1.21 \text{ in.}$$

$$M_{lt} = HL$$
$$= (20 \text{ kips})(15 \text{ ft})$$
$$= 300 \text{ kip-ft}$$

$$P_r = P_A$$
$$= 200 \text{ kips}$$

$$\frac{P_r}{P_c} = 0.200$$

From AISC *Manual* Table 3-10, the available flexural strength, ϕM_n, is

$$\phi M_n = 573 \text{ kip-ft}$$
$$P_{ns} = A_g F_y$$
$$= (26.5 \text{ in.}^2)(50 \text{ ksi})$$
$$= 1{,}330 \text{ kips}$$

The axial load ratio is:

$$\frac{\alpha P_r}{P_{ns}} = \frac{(1.00)(200 \text{ kips})}{1{,}330 \text{ kips}}$$
$$= 0.15$$

Because $\frac{\alpha P_r}{P_{ns}} < 0.5$, τ_b is 1.0 and the IAM amplifier is obtained from Equation 15

$$B_3 = \frac{4}{5 - B_2} \quad (15)$$
$$= \frac{4}{5 - 1.21}$$
$$= 1.06$$

Table A1. Interaction Demand-to-Capacity Ratios for Different Methods of Design for Stability	
Method	**Value**
First-order (FOM)	0.811
Second-order (ELM)	0.840
Simplified ELM	0.966
Direct analysis (DM)	0.796
Indirect analysis (IAM)	0.796

The IAM moment is:

$$\begin{aligned} M_r &= B_2 B_3 M_{lt} \\ &= (1.21)(1.06)(300 \text{ kip-ft}) \\ &= 385 \text{ kip-ft} \end{aligned}$$

Because $P_r/P_c \geq 0.2$, AISC *Specification* Equation H1-1a applies:

$$\begin{aligned} \frac{P_r}{P_c} + \frac{8}{9}\left(\frac{M_r}{\phi M_n}\right) &= 0.200 + \frac{8}{9}\left(\frac{385 \text{ kip-ft}}{573 \text{ kip-ft}}\right) \\ &= 0.796 \end{aligned} \qquad \text{(Spec. Eq. H1-1a)}$$

Table A1 shows the interaction equation values from Carter and Geschwindner for the FOM, ELM, simplified ELM, and DM using AISC *Specification* Equation H1-1a. The table adds the IAM value computed above, which precisely matches the DM for this simple system.

APPENDIX B

VERIFICATION: CANTILEVER STABILITY COLUMN WITH LEANING COLUMN (PARAMETRIC STUDY)

To verify that the proposed IAM produces forces consistent with the DM over a broad range of multiple parameters, the results of calculations similar to those in Appendix A are presented here in tabular form. These examples use a frame of the same configuration as that in Appendix A (Figure A1), analyzed using first-order analysis, second-order analysis, and DM (second-order analysis with modified stiffness properties). The stability column is an ASTM A992 W12×120 oriented in the strong axis and restrained from lateral torsional buckling along its length such that the flexural strength is based on the plastic section modulus ($\phi M_n = \phi M_p$ = 9,300 kip-in.). The column is restrained from minor-axis buckling at the top and bottom. The LRFD method is employed in this example.

Several cases were studied, covering a range of second-order effects and axial-force demands on the stability column and multiple frame heights. The analyses were conducted using formulae for flexural stiffness and do not include shear deformations. The method was confirmed using analysis software and benchmark problems. Using formulae permits a systematic tabular comparison of results from DM and IAM evaluations varying multiple parameters in a spreadsheet.

Following methods developed by LeMessurier (1977), second-order effects incorporate either a force-amplification factor, F_{AF}, or a displacement amplification factor, D_{AF}. Nomenclature and equations for these factors correspond to those used by Griffis and White (2013).

The force amplification factor is presented in Equation A-9 in Griffis and White (2013):

$$F_{AF} = \frac{1}{1 - \dfrac{\sum P}{P_L - \sum C_L P}} \tag{21}$$

where

C_L = factor that accounts for the reduction in column sidesway stiffness due to the presence of axial load on the column

P = applied vertical force, kips

P_L = story lateral force required to induce a first-order unit drift, kips

ΣP = sum of applied vertical forces, kips

In the example frame, the vertical force is:

$$\sum P = P_A + P_B \tag{22}$$

For a cantilever column, the parameter P_L is:

$$P_L = \frac{3EI}{L^2} \tag{23}$$

The factor C_L is zero for columns not providing lateral stiffness. For the cantilever column C_L is:

$$C_L = \left(\frac{12}{\pi^2} - 1\right)\left(\frac{\beta_L}{3 + 9\alpha}\right)^2 \tag{24}$$

where

α = ratio of the smaller to the larger end moment in the moment-frame column, determined from a first-order sidesway analysis

= 0 for a cantilever column

β_L = coefficient corresponding to the contribution of the moment-frame column to the first-order story sidesway stiffness

= 3 for a cantilever column

Thus, for the frame under consideration:

$$F_{AF} = \frac{1}{1 - \dfrac{P_A + P_B}{3EI/L^2 - \left(\dfrac{12}{\pi^2} - 1\right)P_A}} \tag{25}$$

For the DM, the stiffness term is reduced by $0.8\tau_b$:

$$F_{AF-DM} = \frac{1}{1 - \dfrac{P_A + P_B}{0.8\tau_b\, 3EI/L^2 - \left(\dfrac{12}{\pi^2} - 1\right)P_A}} \tag{26}$$

The displacement amplification factor D_{AF} is presented in Equation A-10 in Griffis and White (2013):

$$D_{AF} = \frac{1}{1 - \dfrac{\sum P + \sum C_L P}{P_L}} \tag{27}$$

For the frame under consideration:

$$D_{AF} = \frac{1}{1 - \dfrac{\dfrac{12}{\pi^2} P_A + P_B}{3EI/L^2}} \tag{28}$$

For the DM the stiffness term is reduced by $0.8\tau_b$:

$$D_{AF-DM} = \frac{1}{1 - \dfrac{12/\pi^2 \, P_A + P_B}{0.8\tau_b \, 3EI/L^2}} \tag{29}$$

Moments are determined as follows:

$$M_{FOA} = HL \tag{30}$$

$$M_{SOA} = F_{AF} HL \tag{31}$$

$$M_{DM} = F_{AF-DM} HL \tag{32}$$

Displacements are determined as follows:

$$\Delta_1 = \frac{HL^3}{3EI} \tag{33}$$

$$\Delta_2 = D_{AF} \Delta_1 \tag{34}$$

$$\Delta_{DM} = D_{AF-DM} \Delta_1 \tag{35}$$

Table B1 provides a systematic comparison of DM and IAM demand-to-capacity ratios for varying column height, axial load ratios ($\alpha P_r/P_{ns}$), and second-order effects (B_2). The table shows the analysis and loading information and calculated τ_b factors for the stability column, as well as notional loads where there is no applied lateral load and where the B_2 factor is greater than 1.5. The table also shows the results, including analyzed first-order and second-order displacement (Δ_1 and Δ_2), the second-order displacement corresponding to the DM (Δ_{DM}), and analyzed first-order, second-order, and DM moments (M_{FOA}, M_{SOA}, and M_{DM}).

Table B1 shows factors B_2 and B_3 determined in two ways. First, B_2 is calculated using Equation 12, and the corresponding value of B_3 is determined using Equation 14. Second, a value of B_2' is calculated as the ratio of Δ_2 to Δ_1 from the analysis (Equation 16), and the corresponding value of B_3' is determined (Equation 17). The table presents the F_{AF} and D_{AF} factors (Equations 25–29), and the amplifier products B_2B_3 and $B_2'B_3'$ for comparison.

The table shows calculated demand-to-capacity ratios for the stability column using Chapter H interaction equations from the AISC *Specification* for DM, IAM (using B_3), and IAM′ (using B_3') forces. Frame heights were selected to provide a range of stability column slenderness. Gravity loads were selected to achieve target values of B_2, and to provide both high- and low-axial-stress cases. Lateral loads were selected such that the DM produced demand-to-capacity ratios of 1.00 (as shown in the DCR column).

Cases B1–B4 [at the top of the table) are the results from Benchmark Problem Case 2 in AISC *Specification* Figure C-C2.3 (AISC, 2016)], neglecting shear deformations. Results confirm that accurate moments and displacements are obtained using the formulae in the table.

Cases 1–6 cover a range of B_2 from 1.11 to 1.61 with high axial-force in the stability column such that $\alpha P_r/P_{ns} = 0.7$ and $\tau_b = 0.84$. (The very low slenderness permits such high force.) The stability column has $P_A/P_{e1} = 0.10$ (where P_{e1} is the Euler buckling load

determined in the plane of bending per AISC *Specification* Equation A-8-5). The system reaches the "limit of stability" (i.e., a demand-to-capacity ratio of 1.0 under vertical and notional loads alone with no applied lateral force) at $B_2 = 1.61$.

Cases 7–17 cover a range of B_2 from 1.10 to 3.00 with no axial force in the stability column, which has low slenderness.

Cases 18–20 cover a range of B_2 from 1.5 to 1.82 with high axial force in the low-slenderness stability column such that $\tau_b = 0.89$. Because of the high stability-column axial force and column height, lower values of B_2 cannot be achieved. The stability column has $P_A/P_{e1} = 0.34$. The system reaches the limit of stability at $B_2 = 1.82$.

Cases 21–28 cover a range of B_2 from 1.40 to 3.00 with moderate axial force in the moderate-slenderness stability column, which has $P_A/P_{e1} = 0.29$.

Cases 29–38 are similar to cases 21–28 and cover a range of B_2 from 1.10 to 3.00. This range of B_2 is achieved by varying the stability-column axial force rather than the leaning-column axial force.

Cases 39–44 are similar to case 34. Both P_A and P_B are varied such that $B_2 = 2.00$ is maintained for a range of P_A/P_{e1} from 0.09 to 0.52.

Cases 45–50 vary both P_A and P_B such that $B_2 = 2.00$ is maintained for a range of slenderness (L/r) from 64 to 383.

Table B1 can be used to assess the correspondence of the IAM to the DM using both the design moments obtained and the design interaction value from AISC *Specification* Section H1.1 (AISC, 2016). Comparison of the moments provides a measure of the accuracy of the IAM. However, in cases where the axial load in the stability column is large, the moment represents a small contribution to the design interaction ratio, and thus differences in moment are of less consequence. Demand-to-capacity ratios differing from 1.00 are highlighted in the table, as are ratios of amplified moments to DM moments differing from 1.00.

Comparison of Moments

The table presents three moment ratios:

- Amplified first-order moment to DM moment ($B_2B_3M_{FOA}/M_{DM}$).
- Amplified second-order moment to DM moment (B_3M_{SOA}/M_{DM}).
- Amplified second-order moment to DM moment ($B_3' M_{SOA}/M_{DM}$) based on analyzed displacements.

Ratios above 1.00 indicate that the IAM is conservative, while ratios below 1.00 indicate the opposite. The results indicate that use of the IAM with amplifiers B_2' and B_3' based on analyzed second-order displacements is always conservative in the range studied. Use of first-order analysis with amplifiers B_2 and B_3 based on first-order displacements is conservative for $B_2 \leq 2.5$. Second-order analysis with the amplifier B_3 based on first-order displacements is conservative for $B_2 \leq 2.0$. For cases with $B_2 \geq 2.0$ and $P_A/P_{e1} \geq 0.29$, use of the amplifier B_3 based on first-order displacements becomes slightly unconservative. As noted by Surovek-Maleck and White (2004), the approximate methods of second-order analysis may become less reliable as column P_A/P_{e1} increases.

Comparison of Interaction Ratios

Comparison of interaction ratios was limited to IAM using second-order analysis; amplified first-order analysis forces were not evaluated. Interaction ratios were evaluated for the DM, the IAM, and the IAM′ (using the amplifiers B_3' based on analyzed second-order displacements). (Horizontal forces were selected to produce DM demand-to-capacity ratios of 1.00.) Cases in which the IAM demand-to-capacity ratio is greater than 1.00 indicate that the IAM is conservative compared to the DM; cases in which the IAM demand-to-capacity ratio is less than 1.00 indicate that the IAM is unconservative. Cases in which the IAM produces an unconservative demand-to-capacity ratio by more than 0.005 are outside the range of proposed applicability. In short, the IAM matches the DM or is slightly conservative for $B_2 \leq 2.0$. Above that range, B_3 (which is a function of B_2) could be unconservative as B_2 deviates slightly from Δ_2/Δ_1. Based on the results, use of the IAM is conservative for $B_2 \leq 2.0$ and use of the IAM′ (which utilizes B_3' from Equation 17) is always conservative in the range studied.

Table B1. Verification Analysis Summary

	L (in.)	L/r	H (kips)	N (kips)	P_A (kips)	τ_b	P_A/P_{e1}	P_B (kips)	P_{story} (kips)	R_M	B_2	B_3	B_2B_3	F_{AF}	$F_{AF\text{-}DM}$	D_{AF}	$D_{AF\text{-}DM}$
Notes	**1**		**2**	**3**	**4**	**5**	**6**	**7**	**8**	**9**	**10**	**11**	**12**	**13**	**14**	**15**	**16**
Case																	
B1	336	176	1.0	0.0	0	1.00	0.00	0	0	1.00	1.00			1.00		1.00	
B2	336	176	1.0	0.0	100	1.00	0.33	0	100	0.85	1.46			1.40		1.48	
B3	336	176	1.0	0.0	150	1.00	0.49	0	150	0.85	1.90			1.79		1.96	
B4	336	176	1.0	0.0	200	1.00	0.65	0	200	0.85	2.71			2.54		2.87	
1	80	26	21.0	0.0	1232	0.84	0.10	0	1,232	0.85	1.11	1.06	1.17	1.09	1.15	1.11	1.18
2	80	26	18.1	0.0	1232	0.84	0.10	991	2,223	0.92	1.20	1.11	1.33	1.18	1.31	1.21	1.34
3	80	26	16.0	0.0	1232	0.84	0.10	1,928	3,160	0.94	1.30	1.17	1.52	1.28	1.50	1.31	1.54
4	80	26	14.0	0.0	1232	0.84	0.10	2,730	3,962	0.95	1.40	1.24	1.74	1.38	1.71	1.41	1.76
5	80	26	12.5	0.0	1232	0.84	0.10	3,424	4,656	0.96	1.50	1.32	1.98	1.48	1.96	1.51	2.01
6	80	26	0.0	10.6	1232	0.84	0.10	4,061	5,293	0.97	1.61	1.42	2.28	1.59	2.26	1.62	2.32
7	150	48	55.0	0.0	0	1.00	0.00	376	376	1.00	1.10	1.03	1.13	1.10	1.13	1.10	1.13
8	150	48	49.1	0.0	0	1.00	0.00	690	690	1.00	1.20	1.05	1.26	1.20	1.26	1.20	1.26
9	150	48	44.1	0.0	0	1.00	0.00	955	955	1.00	1.30	1.08	1.41	1.30	1.41	1.30	1.41
10	150	48	39.9	0.0	0	1.00	0.00	1,182	1,182	1.00	1.40	1.11	1.56	1.40	1.56	1.40	1.56
11	150	48	36.2	0.0	0	1.00	0.00	1,379	1,379	1.00	1.50	1.14	1.71	1.50	1.71	1.50	1.71
12	150	48	25.2	3.5	0	1.00	0.00	1,773	1,773	1.00	1.75	1.23	2.15	1.75	2.15	1.75	2.15
13	150	48	19.1	4.1	0	1.00	0.00	2,069	2,069	1.00	2.00	1.33	2.67	2.00	2.67	2.00	2.67
14	150	48	14.4	4.6	0	1.00	0.00	2,299	2,299	1.00	2.25	1.45	3.27	2.25	3.27	2.25	3.27
15	150	48	10.5	5.0	0	1.00	0.00	2,482	2,482	1.00	2.50	1.60	4.00	2.50	4.00	2.50	4.00
16	150	48	7.4	5.3	0	1.00	0.00	2,633	2,633	1.00	2.75	1.78	4.89	2.75	4.89	2.75	4.89
17	150	48	4.8	5.5	0	1.00	0.00	2,758	2,758	1.00	3.00	2.00	6.00	3.00	6.00	3.00	6.00
18	150	48	5.0	0.0	1172	0.89	0.34	0	1,172	0.85	1.50	1.25	1.88	1.43	1.77	1.53	1.94
19	150	48	0.6	3.2	1172	0.89	0.34	403	1,575	0.89	1.75	1.44	2.51	1.68	2.41	1.79	2.64
20	150	48	0.0	3.3	1172	0.89	0.34	500	1,672	0.89	1.82	1.50	2.73	1.76	2.64	1.87	2.89
21	300	96	16.3	0.0	250	1.00	0.29	1.4	251	0.85	1.40	1.11	1.56	1.34	1.48	1.42	1.58
22	300	96	14.7	0.0	250	1.00	0.29	52	302	0.88	1.50	1.14	1.71	1.45	1.64	1.52	1.75
23	300	96	10.8	0.8	250	1.00	0.29	152	402	0.91	1.75	1.23	2.15	1.70	2.08	1.79	2.23
24	300	96	8.3	1.0	250	1.00	0.29	226	476	0.92	2.00	1.33	2.67	1.95	2.60	2.05	2.79
25	300	96	6.4	1.1	250	1.00	0.29	284	534	0.93	2.25	1.45	3.27	2.20	3.23	2.32	3.46
26	300	96	4.9	1.2	250	1.00	0.29	330	580	0.94	2.50	1.60	4.00	2.45	4.01	2.59	4.29
27	300	96	3.6	1.2	250	1.00	0.29	368	618	0.94	2.75	1.78	4.89	2.71	4.98	2.86	5.33
28	300	96	2.6	1.3	250	1.00	0.29	400	650	0.94	3.00	2.00	5.99	2.96	6.24	3.13	6.67
29	300	96	26.6	0.0	80	1.00	0.09	0	80	0.85	1.10	1.03	1.13	1.09	1.11	1.10	1.13
30	300	96	23.0	0.0	147	1.00	0.17	0	147	0.85	1.20	1.05	1.26	1.17	1.23	1.21	1.27
31	300	96	19.4	0.0	203	1.00	0.24	0	203	0.85	1.30	1.08	1.41	1.26	1.35	1.31	1.42
32	300	96	13.7	0.0	293	1.00	0.34	0	293	0.85	1.50	1.14	1.71	1.43	1.62	1.53	1.76
33	300	96	8.5	0.8	377	1.00	0.44	0	377	0.85	1.75	1.23	2.15	1.65	2.02	1.80	2.24
34	300	96	5.5	0.9	440	1.00	0.52	0	440	0.85	2.00	1.33	2.67	1.88	2.50	2.07	2.82
35	300	96	3.5	1.0	488	1.00	0.57	0	488	0.85	2.25	1.45	3.27	2.11	3.09	2.35	3.54
36	300	96	2.1	1.1	528	1.00	0.62	0	528	0.85	2.50	1.60	4.00	2.34	3.83	2.63	4.45
37	300	96	1.1	1.1	559	1.00	0.66	0	559	0.85	2.75	1.78	4.89	2.58	4.80	2.92	5.62
38	300	96	0.4	1.2	586	1.00	0.69	0	586	0.85	3.00	2.00	6.00	2.82	6.10	3.22	7.21
39	300	96	10.1	1.0	80	1.00	0.09	426	506	0.98	2.00	1.34	2.68	1.99	2.66	2.02	2.72
40	300	96	9.7	1.0	147	1.00	0.17	347	494	0.96	2.00	1.33	2.66	1.97	2.63	2.03	2.74
41	300	96	9.0	1.0	203	1.00	0.24	282	485	0.94	2.00	1.33	2.67	1.96	2.62	2.05	2.77
42	300	96	7.7	0.9	293	1.00	0.34	176	469	0.91	2.00	1.33	2.67	1.93	2.59	2.06	2.80
43	300	96	6.4	0.9	377	1.00	0.44	77	454	0.88	2.00	1.34	2.68	1.91	2.55	2.07	2.83
44	300	96	5.5	0.9	440	1.00	0.52	0	440	0.85	2.00	1.33	2.67	1.88	2.50	2.07	2.82
45	200	64	1.2	2.0	989	0.98	0.52	0	989	0.85	2.00	1.37	2.74	1.88	2.57	2.07	2.91
46	400	128	4.7	0.5	247	1.00	0.52	0	247	0.85	2.00	1.33	2.67	1.88	2.50	2.07	2.82
47	600	192	3.2	0.2	110	1.00	0.52	0	110	0.85	2.00	1.33	2.67	1.88	2.50	2.07	2.82
48	800	256	2.5	0.1	62	1.00	0.52	0	62	0.85	2.00	1.33	2.67	1.88	2.50	2.07	2.82
49	1000	319	2.0	0.1	40	1.00	0.52	0	40	0.85	2.00	1.33	2.67	1.88	2.50	2.07	2.82
50	1200	383	1.7	0.1	27	1.00	0.52	0	27	0.85	2.00	1.33	2.67	1.88	2.50	2.07	2.82
25'	300	96	6.4	1.1	250	1.00	0.29	284	534	0.92	2.29	1.48	3.38	2.20	3.23	2.32	3.46
26'	300	96	4.9	1.2	250	1.00	0.29	330	580	0.92	2.55	1.63	4.16	2.45	4.01	2.59	4.29
27'	300	96	3.6	1.2	250	1.00	0.29	368	618	0.93	2.81	1.82	5.12	2.71	4.98	2.86	5.33
28'	300	96	2.6	1.3	250	1.00	0.29	400	650	0.93	3.07	2.07	6.35	2.96	6.24	3.13	6.67
35'	300	96	3.5	1.0	488	1.00	0.57	0	488	0.82	2.35	1.51	3.54	2.11	3.09	2.35	3.54
36'	300	96	2.1	1.1	528	1.00	0.62	0	528	0.82	2.63	1.69	4.45	2.34	3.83	2.63	4.45
37'	300	96	1.1	1.1	559	1.00	0.66	0	559	0.82	2.92	1.92	5.62	2.58	4.80	2.92	5.62

Table B1. Verification Analysis Summary *(continued)*

Δ_1 (in.)	Δ_2 (in.)	Δ_{DM} (in.)	B'_2	B'_3	$B'_2B'_3$	M_{FOA} (kip-in.)	M_{SOA} (kip-in.)	M_{DM} (kip-in.)	DCR			$B_2B_3M_{FOA}/M_{DM}$	B_3M_{SOA}/M_{DM}	B'_3M_{SOA}/M_{DM}	
									DM	IAM (B_2B_3)	IAM′ (B_3SOA)				
17	18	19	20	21	22	23	24	25	26	27	28	29	30	31	Notes Case
0.90	0.90					336	336								B1
0.90	1.34					336	470								B2
0.90	1.76					336	600								B3
0.90	2.59					336	854								B4
0.12	0.13	0.14	1.11	1.06	1.18	1680	1838	1930	1.00	1.00	1.00	1.02	1.01	1.01	1
0.10	0.12	0.13	1.21	1.11	1.34	1447	1713	1888	1.00	1.00	1.00	1.02	1.01	1.01	2
0.09	0.12	0.14	1.31	1.18	1.54	1281	1645	1919	1.00	1.00	1.00	1.02	1.00	1.01	3
0.08	0.11	0.14	1.41	1.25	1.76	1121	1551	1921	1.00	1.00	1.00	1.01	1.00	1.01	4
0.07	0.10	0.14	1.51	1.33	2.01	997	1479	1953	1.00	1.00	1.00	1.01	1.00	1.01	5
0.06	0.09	0.14	1.62	1.43	2.32	847	1346	1910	1.00	1.00	1.00	1.01	1.00	1.01	6
1.99	2.19	2.25	1.10	1.03	1.13	8243	9067	9299	1.00	1.00	1.00	1.00	1.00	1.00	7
1.78	2.14	2.25	1.20	1.05	1.26	7362	8834	9299	1.00	1.00	1.00	1.00	1.00	1.00	8
1.60	2.08	2.25	1.30	1.08	1.41	6618	8603	9301	1.00	1.00	1.00	1.00	1.00	1.00	9
1.45	2.02	2.25	1.40	1.11	1.56	5979	8371	9301	1.00	1.00	1.00	1.00	1.00	1.00	10
1.31	1.97	2.25	1.50	1.14	1.71	5426	8138	9301	1.00	1.00	1.00	1.00	1.00	1.00	11
1.04	1.83	2.25	1.75	1.23	2.15	4318	7556	9300	1.00	1.00	1.00	1.00	1.00	1.00	12
0.84	1.69	2.25	2.00	1.33	2.67	3487	6974	9299	1.00	1.00	1.00	1.00	1.00	1.00	13
0.69	1.55	2.25	2.25	1.45	3.27	2842	6395	9301	1.00	1.00	1.00	1.00	1.00	1.00	14
0.56	1.41	2.25	2.50	1.60	4.00	2326	5814	9303	1.00	1.00	1.00	1.00	1.00	1.00	15
0.46	1.26	2.25	2.75	1.78	4.89	1903	5233	9303	1.00	1.00	1.00	1.00	1.00	1.00	16
0.37	1.12	2.25	3.00	2.00	6.00	1550	4651	9303	1.00	1.00	1.00	1.00	1.00	1.00	17
0.18	0.28	0.35	1.53	1.27	1.94	750	1074	1328	1.00	1.00	1.01	1.06	1.01	1.03	18
0.14	0.24	0.36	1.79	1.47	2.64	563	947	1356	1.00	1.01	1.01	1.04	1.00	1.03	19
0.12	0.23	0.35	1.87	1.54	2.89	502	881	1323	1.00	1.00	1.01	1.04	1.00	1.03	20
4.72	6.70	7.48	1.42	1.12	1.58	4881	6564	7231	1.00	1.01	1.01	1.05	1.01	1.01	21
4.26	6.50	7.48	1.52	1.15	1.75	4408	6370	7231	1.00	1.00	1.01	1.05	1.01	1.01	22
3.36	6.00	7.48	1.79	1.25	2.23	3472	5886	7231	1.00	1.00	1.01	1.03	1.00	1.01	23
2.68	5.51	7.48	2.05	1.36	2.79	2777	5402	7231	1.00	1.00	1.01	1.02	1.00	1.01	24
2.16	5.01	7.48	2.32	1.49	3.46	2237	4915	7231	1.00	0.99	1.01	1.01	0.99	1.01	25
1.75	4.51	7.48	2.59	1.66	4.29	1805	4425	7231	1.00	0.99	1.01	1.00	0.98	1.01	26
1.40	4.01	7.48	2.86	1.87	5.33	1452	3931	7231	1.00	0.98	1.01	0.98	0.97	1.01	27
1.12	3.50	7.48	3.13	2.13	6.67	1159	3435	7231	1.00	0.96	1.01	0.96	0.95	1.01	28
7.70	8.50	8.73	1.10	1.03	1.13	7969	8648	8841	1.00	1.00	1.00	1.02	1.00	1.00	29
6.67	8.06	8.50	1.21	1.05	1.27	6901	8082	8458	1.00	1.01	1.01	1.03	1.01	1.01	30
5.62	7.38	8.00	1.31	1.08	1.42	5810	7307	7840	1.00	1.01	1.01	1.04	1.01	1.01	31
3.98	6.07	6.99	1.53	1.15	1.76	4115	5893	6674	1.00	1.01	1.01	1.06	1.01	1.02	32
2.68	4.80	6.00	1.80	1.25	2.24	2768	4578	5592	1.00	1.00	1.01	1.07	1.01	1.02	33
1.85	3.82	5.22	2.07	1.36	2.82	1912	3593	4780	1.00	1.00	1.01	1.07	1.00	1.03	34
1.30	3.05	4.60	2.35	1.51	3.54	1342	2831	4149	1.00	1.00	1.01	1.06	0.99	1.03	35
0.92	2.42	4.09	2.63	1.69	4.45	950	2226	3644	1.00	0.99	1.01	1.04	0.98	1.03	36
0.65	1.90	3.66	2.92	1.92	5.62	673	1736	3231	1.00	0.99	1.01	1.02	0.96	1.03	37
0.46	1.47	3.30	3.22	2.24	7.21	473	1335	2887	1.00	0.98	1.01	0.98	0.92	1.04	38
3.21	6.50	8.73	2.02	1.34	2.72	3320	6607	8841	1.00	1.00	1.00	1.00	1.00	1.00	39
3.11	6.31	8.50	2.03	1.35	2.74	3213	6327	8458	1.00	1.00	1.01	1.01	1.00	1.01	40
2.89	5.91	8.00	2.05	1.35	2.77	2989	5855	7840	1.00	1.00	1.01	1.02	1.00	1.01	41
2.49	5.13	6.99	2.06	1.36	2.80	2578	4986	6674	1.00	1.00	1.01	1.03	1.00	1.02	42
2.12	4.39	6.00	2.07	1.37	2.83	2191	4183	5592	1.00	1.00	1.01	1.05	1.00	1.02	43
1.85	3.82	5.22	2.07	1.36	2.82	1912	3593	4780	1.00	1.00	1.01	1.07	1.00	1.03	44
0.27	0.56	0.79	2.07	1.40	2.91	632	1187	1622	1.00	1.00	1.00	1.07	1.00	1.03	45
3.54	7.32	9.99	2.07	1.36	2.82	2058	3868	5145	1.00	1.00	1.01	1.07	1.00	1.03	46
7.98	16.52	22.54	2.07	1.36	2.82	2064	3879	5160	1.00	1.00	1.01	1.07	1.00	1.03	47
14.21	29.40	40.13	2.07	1.36	2.82	2067	3885	5168	1.00	1.00	1.01	1.07	1.00	1.03	48
22.23	45.99	62.77	2.07	1.36	2.82	2069	3889	5174	1.00	1.00	1.01	1.07	1.00	1.03	49
32.02	66.26	90.43	2.07	1.36	2.82	2070	3890	5176	1.00	1.00	1.02	1.07	1.00	1.03	50
2.16	5.02	7.48	2.32	1.49	3.46	2238	4917	7233	1.00	1.00	1.01	1.05	1.00	1.01	25′
1.75	4.52	7.48	2.59	1.66	4.29	1806	4427	7235	1.00	1.00	1.01	1.04	1.00	1.01	26′
1.41	4.01	7.49	2.86	1.87	5.33	1454	3935	7240	1.00	1.00	1.01	1.03	0.99	1.01	27′
1.12	3.49	7.45	3.13	2.13	6.67	1155	3422	7204	1.00	0.99	1.01	1.02	0.98	1.01	28′
1.30	3.05	4.60	2.35	1.51	3.54	1342	2831	4149	1.00	1.01	1.01	1.15	1.03	1.03	35′
0.92	2.42	4.09	2.63	1.69	4.45	950	2226	3644	1.00	1.01	1.01	1.16	1.03	1.03	36′
0.65	1.90	3.66	2.92	1.92	5.62	673	1736	3231	1.00	1.01	1.01	1.17	1.03	1.03	37′

Notes for Table B1:

1. Cantilever height. Darker values are larger.
2. Horizontal load selected to produce demand-to-capacity ratio of 1.0 for the IAM. Darker values are larger within each group.
3. Notional load N determined using Equation 18.
4. Axial force in the stability column. Darker values are larger within each group.
5. The τ_b parameter for the stability column determined using Equation 3. Values less than 1.0 are highlighted.
6. The ratio for the stability column, with the Euler buckling load P_{e1} determined in the plane of bending per AISC *Specification* Equation A-8-5. Darker values are larger.
7. Axial force in the leaning column. Darker values are larger within each group.
8. The sum of the axial forces on the stability column and on the leaning column ($P_{story} = P_A + P_B$).
9. $R_M = 1 - 0.15P_A/P_{story}$, AISC *Specification* Equation A-8-8. Darker values are smaller.
10. The B_2 factor determined using Equation 12. Darker values are larger.
11. The B_3 factor determined using Equation 13. Darker values are larger.
12. Product of B_2 and B_3. Darker values of B_2 are larger.
13. Force amplification factor using Equation 25.
14. Force amplification factor for DM using Equation 26.
15. Displacement amplification factor using Equation 28.
16. Displacement amplification factor for DM using Equation 29.
17. First-order displacement, Δ_1, determined using Equation 33.
18. Second-order displacement, Δ_2, determined using Equation 34.
19. Second-order displacement using DM, Δ_{DM}, determined using Equation 35.
20. Ratio of second-order to first-order displacements (Equation 16).
21. The B'_3 factor determined using Equation 17.
22. Product of B'_2 and B'_3.
23. First-order overturning moment M_{FOA} determined using Equation 30.
24. Second-order overturning moment M_{SOA} determined using Equation 31.
25. Second-order overturning moment for DM M_{DM} determined using Equation 32.
26. Stability-column interaction check using AISC *Specification* Equations H1-1a and H1-1b, using *P*A and M_{DM}. Values are 1.00 because the lateral force H is selected to produce this value.
27. Stability-column interaction check using AISC *Specification* Equations H1-1a and H1-1b, using P_A and B_3M_{SOA}.
28. Stability-column interaction check using AISC *Specification* Equations H1-1a and H1-1b, using P_A and B'_3M_{SOA}.
29. Ratio of amplified first-order moment to DM moment ($B_2B_3M_{FOA}/M_{DM}$).
30. Ratio of amplified second-order moment to DM moment (B_3M_{SOA}/M_{DM}).
31. Ratio of amplified second-order moment to DM moment (B'_3M_{SOA}/M_{DM}), Equation 17.

Figure B1 shows demand-to-capacity ratios from selected cases: 21–28, in which the axial force in column B is varied such that there is a range of B_2; 39–44, in which the axial forces in column A and column B are varied such that there is range of axial load ratios P_A/P_{e1} and $B_2 = 2.0$ is maintained; and 29–38, in which the axial force in column A is varied such that there is a range of both P_A/P_{e1} and B_2. The graphs show that for values of $B_2 \leq 2.0$, the IAM can be used to approximate the DM. Above $B_2 = 2.0$, there is the potential for underestimation of demands if the IAM is used with an approximate second-order analysis. Use of the IAM with B'_3 determined using the results of an explicit second-order analysis from Equation 17 does not show this unconservatism for the cases examined.

Based on these results, the IAM provides results consistent with the DM for the range proposed ($B_2 \leq 2.0$).

Reduction of Error by Use of More Exact Formulae

At the bottom of Table B1, cases 25–28 and 35–37 (for which the IAM produced unconservative results for $B_2 > 2.0$) are reanalyzed. (These are presented as cases 25'–28' and 35'–37'.) In these revised cases, a more theoretically correct equation is used for the parameter R_M based on work by LeMessurier (1977):

$$R_M = 1 - \left[1 - \frac{\left(\pi/2\right)^2}{3}\right]\frac{P_A}{P_{Story}} = \frac{\pi^2/12\,P_A + P_B}{P_A + P_B} \tag{36}$$

The results show the unconservative error eliminated for all but one case (28'), in which the unconservative error is reduced to 1% (compared to 3% for case 28). The majority of the error in these cases can therefore be attributed to the simplified equation for R_M in AISC *Specification* Appendix 8, rather than to an inherent deficiency of the IAM.

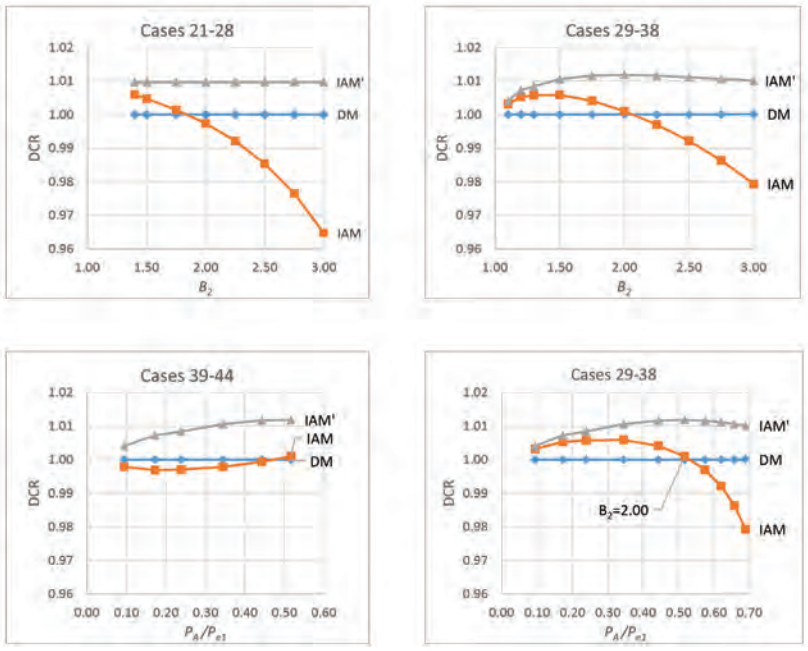

Fig. B1. Selected results from parametric study.

APPENDIX C
EXAMPLE APPLICATION

The following example illustrates the application of the IAM for stability design of a symmetrical eight-story building with moment frames in one direction. Figure C1 shows the plan. The configuration and loads were selected to result in relatively high second-order effects for a building of this height. For simplicity, only two load combinations are considered: one with service-level lateral loads and one with strength-level lateral loads. Two-dimensional analyses of one frame (on line D) are performed. The LRFD method is employed in this example.

The relevant design data are presented in Tables C1 (general design information), C2 (drift evaluation information), and C3 (strength evaluation information). Gravity loads and lateral loads are both given for the entire building, with 50% of each being tributary to the frame being designed. (The tributary gravity load includes that resisted by leaning columns.) Loads directly on the moment-frame columns include a large cladding load. For simplicity, vertical and lateral load values are unrealistically uniform. Factors B_2 and B_3 are calculated in advance of any design, assuming the frames have exactly the stiffness required to meet the drift limit for the appropriate lateral loads, including consideration of second-order effects.

Table C2 contains the information used for the serviceability evaluation. Wind loads are based on a uniform pressure of 14.33 psf, and a tall parapet is assumed, resulting in identical wind forces at each story. (Seismic loads are not considered.) The serviceability drift limit is $L/400$; this is a limit on the second-order drift. The required stiffness is the first-order stiffness that will result in the desired second-order drift (the drift limit) in the presence of the vertical loads. (See note 3. The derivation of this required stiffness which is too large to include in this example.) This required stiffness is used to compute the first-order drift Δ_1, which is then used to compute B_2. Although second-order effects are addressed in these calculations by means of this determination of required stiffness, no design has yet been performed, and only the predesign information is used.

Similarly, Table C3 is constructed using predesign information. Wind loads are based on a uniform pressure of 21.5 lb/ft^2. The first-order lateral stiffness of the system is assumed to be that determined in Table C2 to meet the drift limit in the presence of the serviceability vertical loads. First-order drifts are computed using that stiffness and strength-level lateral loads. (These values are upper bounds based on the assumption of minimum permissible stiffness for serviceability requirements.) The strength-level amplifiers B_2 are then computed based on the vertical loads considered in the strength evaluation. These B_2 values are then used to determine B_3 values, assuming $\alpha P_r/P_{ns} \leq 0.5$.

A frame is designed and analyzed using analysis software to meet the drift limits in Table C2 with the corresponding vertical and lateral loads. Members are selected (and revised) to result in drifts at or just below the drift limit. Second-order effects are considered, with members appropriately meshed to capture P-δ effects. Results are shown in Table C4. Under "Service," the ratio of the second-order drift under service-level lateral loads is compared to the drift limit; these ratios are reasonably close to 1.0 for most of the stories, indicating a design optimized for drift control. The design is shown in Figure C2. Column sizes shown are repeated for all moment-frame columns.

The frame is then analyzed using the loads from Table C3 for strength and stability; lateral loads are amplified with the maximum value of B_3. Results of the strength and stability evaluation are shown in Table C4. These include the beam and column demand-to-capacity ratios at each story determined using analysis software. As the demand-to-capacity ratios are below 1.0, no redesign is required; member selection to meet drift limits governs the design, and the strength and stability evaluation confirms the acceptability of the design.

The frame is reanalyzed using the DM, and beam and column demand-to-capacity ratios are computed. Additionally, to better understand the simplifications and conservatism of the process employed in this example, B_2' (determined from the analysis using Equation 16) and B_3' (using Equation 17) are presented, although these values are not used in the evaluation.

Table C4 presents the results of these analyses and design evaluations. The results show a reasonably close correlation between the IAM and the DM design checks. Typical of many moment frame buildings, the member sizes are selected to meet the drift limits, and the minor differences in the strength-design demand-to-capacity ratios do not affect the economy of the design. The differences in demand-to-capacity ratios are due to two conservative measures. First, the use of the allowable drift in determining the B_3 amplifier overestimates the value (although it simplifies the design process); this could be avoided by using the analysis-based factor B_3' form, Equation 17. Second, the use of the largest value of B_3 for all stories overestimates the effect at upper stories. Level-by-level application of B_3 (or B_3') could address this, as discussed under "Application."

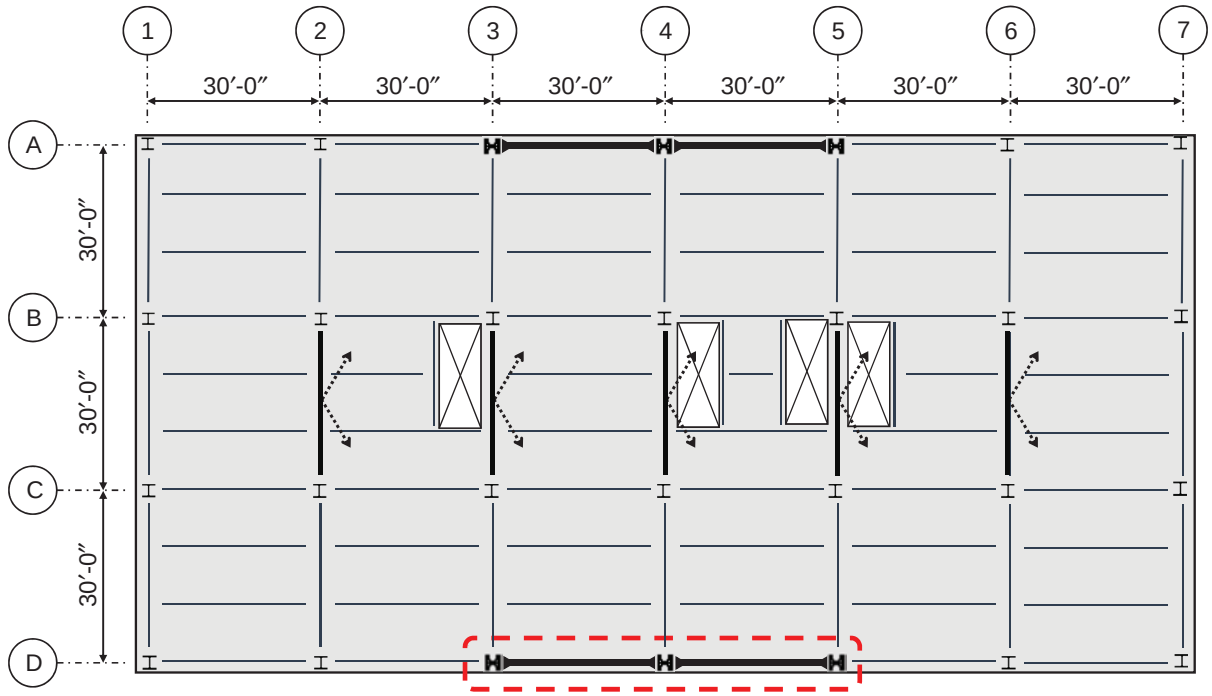

Fig. C1. Typical plan of example building.

Table C1. Pre-Analysis Design Information (General)					
Level	L (in.)	Dead Load (kips)	Live Load (kips)	P_{mf}/P_{story}	R_M
8	180	2000	0	0.275	0.959
7	180	2000	1600	0.275	0.959
6	180	2000	1600	0.275	0.959
5	180	2000	1600	0.275	0.959
4	180	2000	1600	0.275	0.959
3	180	2000	1600	0.275	0.959
2	180	2000	1600	0.275	0.959
1	180	2000	1600	0.275	0.959
Notes		1	1	1	2

Notes:
1. Given information.
2. $R_M = 1 - 0.15P_{mf}/P_{story}$ using AISC *Specification* Equation A-8-8.

Table C2. Pre-Analysis Design Information (Drift Evaluation)						
Level	$H_{service}$ (kips)	$\Delta_{allowable}$ (in.)	P_{story} (kips)	$K_{required}$ (kip/in.)	Δ_1 (in.)	B_2
8	20.0	0.450	2,000	56	0.357	1.26
7	40.0	0.450	4,400	114	0.350	1.29
6	60.0	0.450	6,800	173	0.347	1.30
5	80.0	0.450	9,200	231	0.346	1.30
4	100.0	0.450	11,600	289	0.345	1.30
3	120.0	0.450	14,000	348	0.345	1.30
2	140.0	0.450	16,400	406	0.345	1.31
1	160.0	0.450	18,800	464	0.344	1.31
Notes	1	1	2	3	4	5

Notes.
1. Given information.
2. P_{story} is based on 1.0 times the dead load plus 0.25 times the live load for the service drift check.
3. The required stiffness is based on the lateral load and the drift limit, considering the second-order effect: $K_{required} = H/\Delta_{allowable} + P_{story}/R_M L$.
4. $\Delta_1 = H/K_{required}$
5. The B_2 factor using Equation 12 based on P_{story} for the drift load combination (and on Δ_1 and $H_{service}$).

Table C3. Pre-Analysis Design Information (Strength Evaluation)									
Level	***H* (kips)**	***F* (kips)**	***K*= $K_{required}$ (kip/in.)**	**Δ_1 (in.)**	**P_{story} (kips)**	**B_2**	**θ**	**B_3**	**B_3F (kips)**
8	30	30.0	56	0.535	2,400	1.33	0.24	1.09	33.78
7	60	30.0	114	0.525	5,600	1.40	0.27	1.11	33.78
6	90	30.0	173	0.521	8,800	1.42	0.28	1.12	33.78
5	120	30.0	231	0.519	12,000	1.43	0.29	1.12	33.78
4	150	30.0	289	0.518	15,200	1.44	0.29	1.12	33.78
3	180	30.0	348	0.518	18,400	1.44	0.29	1.12	33.78
2	210	30.0	406	0.517	21,600	1.45	0.30	1.13	33.78
1	240	30.0	464	0.517	24,800	1.45	0.30	**1.13**	33.78
Notes	1	1	2	3	4	5	6	7	8

Notes.
1. Given information.
2. It is conservatively assumed that the stiffness is exactly equal to that required to meet the drift limit.
3. The first-order displacement corresponding to the assumed stiffness and the applied loads.
4. P_{story} is based on 1.2 times the dead load plus 0.5 times the live load for the strength check.
5. The B_2 factor determined using Equation 12 based on P_{story} for the strength load combination.
6. The stability coefficient θ calculated per Equation 1.
7. The B_3 factor determined using Equation 15. The maximum value is highlighted.
8. The amplified forces B_3F to be used in a second-order analysis. The maximum value of B_3 is used at all levels so that overturning effects at lower levels are not underestimated.

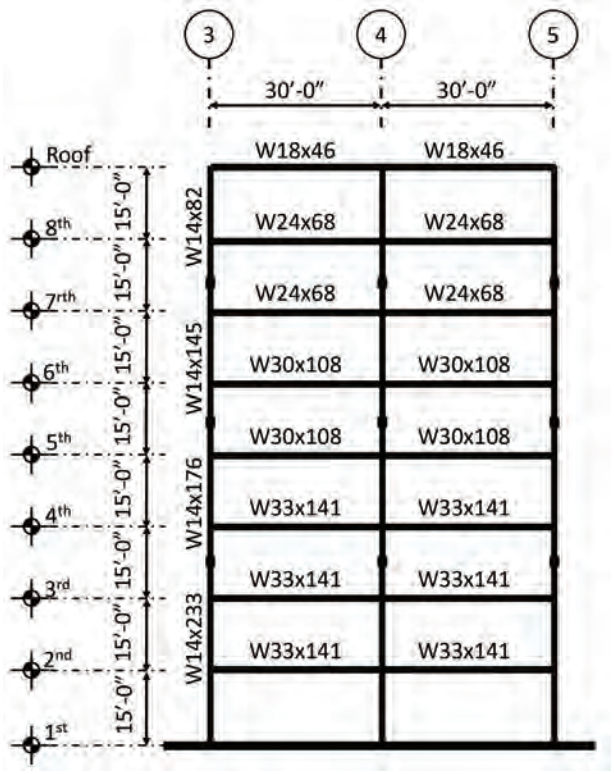

Fig. C2. Moment frame elevation.

Table C4. Analysis Results and Design Checks													
	Service	Strength Evaluation											
								IAM	DM	Ratio	IAM	DM	Ratio
	Δ_2/Δ_{all}	$\alpha P_r/P_{ns}$	τ_b	Δ_1 (in.)	Δ_2 (in.)	B'_2	B'_3	Beam (DCR)	Beam (DCR)	IAM/ DM	Column (DCR)	Column (DCR)	IAM/ DM
Level													
8	0.61	0.07	1.00	0.39	0.49	1.25	1.07	0.13	0.12	1.06	0.14	0.14	1.04
7	0.96	0.16	1.00	0.59	0.79	1.35	1.10	0.21	0.20	1.04	0.45	0.45	1.01
6	0.89	0.15	1.00	0.54	0.74	1.36	1.10	0.31	0.30	1.02	0.25	0.25	1.02
5	0.95	0.21	1.00	0.57	0.79	1.38	1.11	0.27	0.27	1.02	0.45	0.45	1.01
4	0.93	0.22	1.00	0.56	0.78	1.39	1.11	0.32	0.31	1.02	0.47	0.47	1.01
3	1.00	0.28	1.00	0.60	0.84	1.41	1.11	0.29	0.29	1.01	0.58	0.58	1.01
2	0.93	0.25	1.00	0.56	0.78	1.38	1.11	0.33	0.32	1.01	0.50	0.50	1.01
1	0.72	0.29	1.00	0.45	0.59	1.32	1.09	0.33	0.32	1.03	0.65	0.64	1.02
Notes	1	2	3	4	5	6	7	8	9	10	11	12	13

Notes.

1. Second-order serviceability drift divided by drift limit.
2. Gridline 5 column $\alpha P_r/P_{ns}$ ratio.
3. Gridline 5 column τ_b parameter.
4. Δ_1 from a first-order analysis using strength-level loads.
5. Δ_2 from a second-order analysis using strength-level loads.
6. The B'_2 factor determined using Equation 16 based on Δ_1 and Δ_2 from the analysis.
7. The B'_3 factor determined using Equation 17 based on B'_2.
8. Beam demand-to-capacity ratio from IAM second-order analysis amplified by B_3 using AISC *Specification* Equations H1-1a and H1-1b axial-flexure interaction equations.
9. Beam demand-to-capacity ratio from DM second-order analysis with reduced stiffness using AISC *Specification* Equations H1-1a and H1-1b axial-flexure interaction equations.
10. Ratio of IAM to DM beam demand-to-capacity ratio.
11. Gridline 5 column demand-to-capacity ratio from IAM second-order analysis amplified by B_3 using AISC *Specification* Equations H1-1a and H1-1b axial-flexure interaction equations.
12. Gridline 5 column demand-to-capacity ratio from DM second-order analysis with reduced stiffness using AISC *Specification* Equations H1-1a and H1-1b axial-flexure interaction equations. *H* is used for the lateral load.
13. Ratio of IAM to DM gridline 5 column demand-to-capacity ratio.

Steel Structures Research Update

Self-Centering Column Base Connections with Friction Dampers

JUDY LIU

INTRODUCTION

Recent work on a self-centering column base connection with friction dampers is highlighted. This research is a collaborative effort by Senior Researcher Massimo Latour and Professor Gianvittorio Rizzano from the University of Salerno, Italy, and Professors Aldina Santiago and Luis Simões da Silva of the University of Coimbra, Portugal. The work builds off the researchers' combined expertise on "free from damage" beam-to-column connections, friction materials for supplemental damping, and experimental testing and analytical modeling of a variety of connections.

Self-centering and rocking column bases have captured the interest of researchers across the globe. Some of the self-centering column base research in the past decade has originated from Japan, China, the United Kingdom, Taiwan, Canada, and the United States. Hayashi et al. (2018) developed a self-centering, rocking composite frame with post-tensioned (PT), concrete-filled tube (CFT) columns combined with a moment-resisting frame (MRF) with low-yield (LY) fuses. Kamperidis et al. (2018) proposed a partial-strength, self-centering steel column base with post-tensioning and replaceable, hourglass steel yielding devices. Freddi et al. (2017) and Chen et al. (2014) investigated rocking, PT column bases with friction devices to dissipate energy. PT column bases with yielding, buckling restrained steel (BRS) plates have been developed for CFT and wide-flange columns in MRFs (Wang et al., 2019; Chi and Liu, 2012, respectively). The PT column bases studied by Chi and Liu (2012) were part of a larger effort; Sause et al. (2010) conducted extensive design and validation of self-centering moment resisting frames and concentrically braced frames. Wiebe et al. (2013) investigated controlled rocking steel frames with configurations that implement rocking at upper sections to accommodate higher modes. Rocking steel-braced frames using post-tensioning and replaceable seismic fuses were developed by Eatherton et al. (2014).

The Salerno-Coimbra team has developed an alternative self-centering column base solution to minimize initial costs and economic losses. Specific objectives are to limit damage and residual drifts, with connection components that are easy to repair or replace if needed. The self-centering column base has been validated through quasi-static cyclic testing and pseudo-dynamic testing. The self-centering connection has also been investigated through numerical time-history analyses of moment-resisting frames comparing conventional, fixed column bases to self-centering column bases. Some highlights of the research are presented.

Judy Liu, PhD, Research Editor of the AISC Engineering Journal, Professor, Oregon State University, School of Civil and Construction Engineering, Corvallis, Ore. Email: judy.liu@oregonstate.edu

BACKGROUND AND MOTIVATION

The research is focused on design of steel moment-resisting frames (MRFs) to achieve seismic performance objectives while minimizing economic losses. The traditional design strategy is to develop plastic hinges in the beam ends and at the column bases with strong columns and full-strength connections. This strategy results in significant damage and residual drift due to the permanent, plastic deformations. Given the associated costs and questions related to reparability of the structure, the researchers sought alternative energy dissipation methods and connection designs.

With the goal of minimizing damage, the researchers explored partial strength connections with friction dampers. These types of connections were initially proposed by Grigorian et al. (1993). This work was followed by numerous other theoretical, experimental, and numerical studies (Latour et al., 2019). Specifically, in New Zealand, researchers developed the sliding hinge joint (SHJ) (e.g., Khoo et al., 2012; Ramhormozian et al., 2014) for a beam to column connection. The SHJ has a friction connection at the bottom beam flange, with friction pads made of mild steel, aluminum, brass, or abrasion-resistant steel. A European adaptation of this connection uses a bolted T-stub at the top flange and a shop-assembled friction damping device bolted to the bottom flange (Latour et al., 2018). As shown in Figure 1, the friction damping device consists of a slotted haunch; friction pads; L-stubs to connect the haunch to the column; and pretensioned bolts clamping the haunch, friction pads, and L-stubs. Energy dissipation is achieved through slip at the friction pads as the beam rotates about the stem of the T-stub. The same principles can be further adapted for use at a column base.

The success with the adapted sliding hinge connection is tempered by residual drift issues. Although the friction connection does not experience the same damage as a plastic hinge, the connection experiences similar permanent deformations due to its high unloading stiffness. "Indeed, although these connections are very effective from the point of view of the damage avoidance, they still provide significant problems related to the low self-centering capacity." (Latour et al., 2019) To address this, the researchers also explored a supplemental self-centering solution for the column base.

As briefly described earlier, a number of researchers have proposed self-centering and rocking column base solutions. The Salerno–Coimbra team evaluated the various solutions in the development of their own column base. The team looked first to low-damage friction connections developed and tested by Borzouie et al. (2015) and shown to avoid problems with axial shortening of columns due to yielding and local buckling (MacRae et al., 2009). Then, for self-centering solutions, the researchers acknowledged the benefits of using long PT bars extending into the basement level to avoid yielding of those PT bars (e.g., Chi and Liu, 2012), but they suspected difficulties in repair and replacement. The researchers also noted a related objective to avoid any connection of the PT bars to a concrete foundation. Meanwhile, the researchers found promise in a study utilizing a tension-limiting base level hinge. The base hinge consisted of prestressed Ringfeder springs and vertical friction plates. The Ringfeder springs were prestressed by a tightened bolt through their center, and the friction plates did not engage until the gravity load and Ringfeder spring prestress was exceeded (Gledhill et al., 2008). These and additional studies are described in more detail in Latour et al. (2019). From those studies, the researchers proposed to "keep the layout of the connection as simple as possible providing, other than the self-centering capacity, additional benefits such as the absence of interaction with the concrete foundation and the limited size of the connection which is, overall, similar or lower than the size of the cover plates employed to realize a traditional column splice connection" (Latour et al., 2019).

THE PROPOSED COLUMN BASE CONFIGURATION

For their self-centering column base, the researchers propose a column-splice with friction pads and threaded bars with Belleville disk springs, located just above a traditional full-strength base plate connection, as shown in Figure 2(a). The benefits of the proposed connection follow the researchers' objectives of providing a simple, self-centering connection detail that is not larger than a conventional column splice connection and does not have any attachment to the concrete foundation. As such, damage and residual drifts are limited, and the connection components are expected to be easy to repair or replace if needed.

In the proposed self-centering column base, the moment-rotation response is at the column splice and is governed by the component behavior. As shown in Figure 2(a), there is a stiffened base plate connection and a column stub. The column stub is spliced to the rest of the column with flange and web plates and friction pads with pretensioned bolts. Slotted and oversized holes in the column flanges and web above the splice are used to accommodate the rotation—that is, gap opening—at the column flanges. Threaded bars on each side of the column web are anchored to stiffener plates above and below the column splice, with a system of Belleville disk springs between the nuts and stiffener plates. The contributions of the friction pads, threaded bars, and Belleville disk

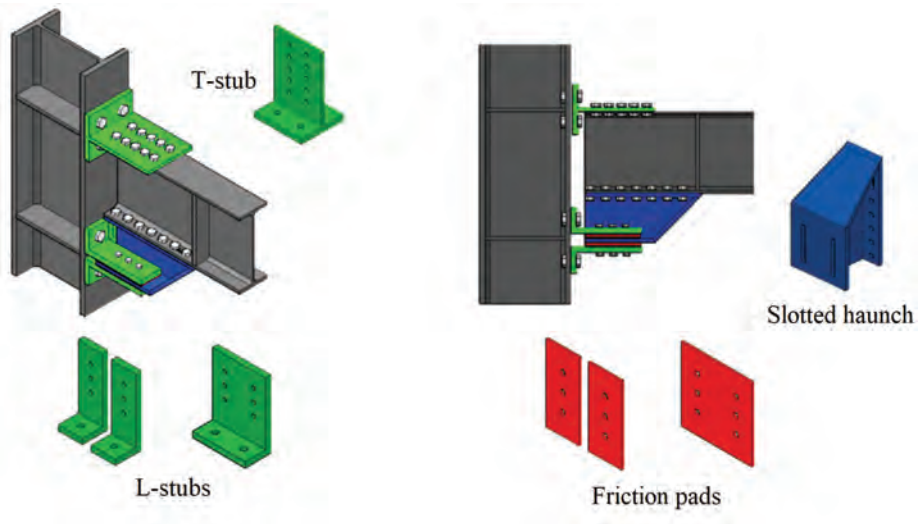

Fig. 1. Beam-to-column connection with friction damping device (based on Latour et al., 2018).

springs to the moment-rotation behavior can be idealized in a mechanical model of equivalent springs, as shown in Figure 2(b). Springs F_w and F_f represent the friction pads on the column web and flanges. The F_w and F_f springs have infinite stiffness up until the slip force and zero stiffness after slip. The translational spring F_{tb} models the axial behavior of the threaded bars, which work in series with the system of disk springs, F_{ds}. The force deformation behavior of the F_{tb} and F_{ds} springs are dependent on the number and properties of the threaded bars and the number and properties of the disk springs working in series and in parallel.

As shown in Figure 3, the disk springs can be stacked to work in parallel or in series, and in this manner, the system of disk springs can be tuned to the desired stiffness. Using the equations developed by Latour et al. (2019) for the equivalent springs, the typical moment-rotation behavior of the connection is shown to follow a flag shape hysteresis, as shown in Figure 2(c). At the bending moment M_0, the initial axial load in the column and the prestress of the threaded bars have been offset, and the bending moment M_1 is the contribution to the bending moment due to the friction pads. At the top of loading branch 1, the moment M_2 represents the decompression moment corresponding to slip in the friction pads and gap opening (i.e., rotation) at the column splice. Loading branch 2 corresponds to slip in the friction pads and loading governed by the stiffnesses of the threaded bars, disk springs, and column in bending. Unloading branches 3 and 4 are governed by the same behavior as the loading branches 1 and 2. The connection returns to zero moment and zero rotation—that is, no residual plastic deformation.

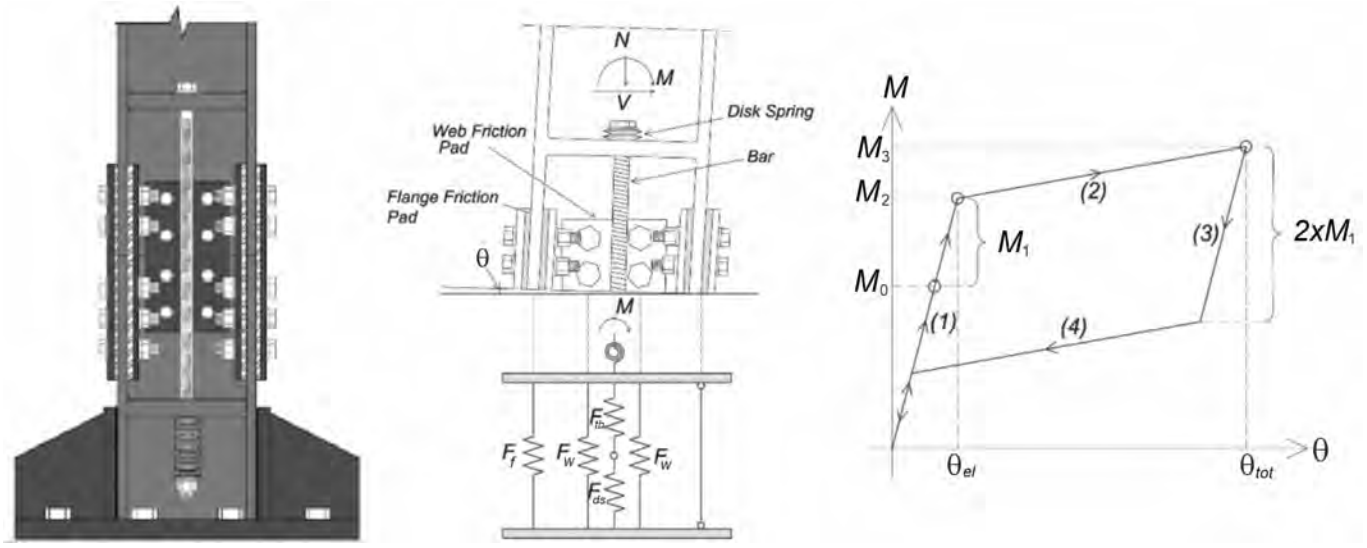

Fig. 2. (a) Connection assembly; (b) mechanical model; (c) theoretical moment-rotation relationship.

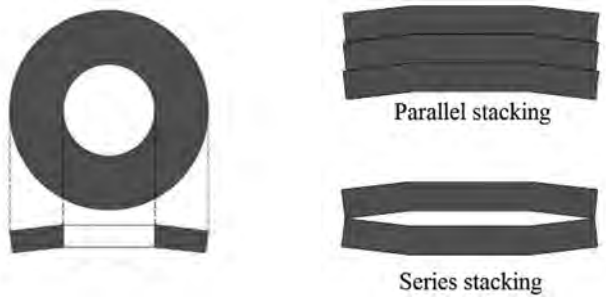

Fig. 3. Belleville disk spring stacking methods.

EXPERIMENTAL INVESTIGATION

The proposed self-centering column base connection has been validated through quasi-static cyclic testing and pseudo-dynamic testing. A cantilever specimen representing the bottom half of a first-story column was designed using the principles outlined in Latour et al. (2019). The column was a 9.44-in.-deep, 9.44-in.-wide H-section (HEB240) with a yield stress of 40 ksi (S275 steel). The connection plates were also S275 steel. The friction pads were S275 steel plates with a 0.012-in. thermal spray aluminum coating. Prior to the cyclic and pseudo-dynamic testing, the friction pads were tested and characterized by Silva (2016).

The test specimens were subjected to axial and lateral loads. As shown in Figure 4, an actuator placed on top of the specimen was used to apply the axial load under load control. A displacement-controlled actuator applied increasing, cyclic lateral displacements at the top of the specimen. Given the limitations of the test equipment, the axial load was limited to 25% of the squash load; from the applied lateral load, the bending moment at the column splice was limited to 95% of the plastic bending moment of the column. Figure 5 shows the test frame, the connection being assembled, and the complete column base before the test.

Cyclic Testing

Four cyclic tests with and without the threaded bars, and with different axial loads, were conducted. Axial loads of 25% or 12.5% of the squash load were applied and held constant for the duration of the test. The test specimens therefore represented an internal moment frame column that does not experience large changes in axial force during an earthquake. For the lower applied axial force, the axial force in the threaded bars, F_{tb}, was increased but could not be increased to the level needed to ensure recentering of the column (Latour et al., 2019).

The cyclic tests validated the design of the self-centering column base connection, highlighting the importance of the recentering bars and the total axial load in the column. Figure 6 compares moment-rotation response—with and without the threaded, recentering bars—for an applied axial load of 25% and 12.5% of the squash load. Both tests with the 25% axial load ratio exhibited self-centering behavior, with residual rotations of 2.1 mrad and 4.1 mrad with and without the recentering bars, respectively. These rotations were both lower than common construction tolerances on the order of 5 mrad (Latour et al., 2019). Figure 6(a) qualitatively shows the improvement in self-centering behavior

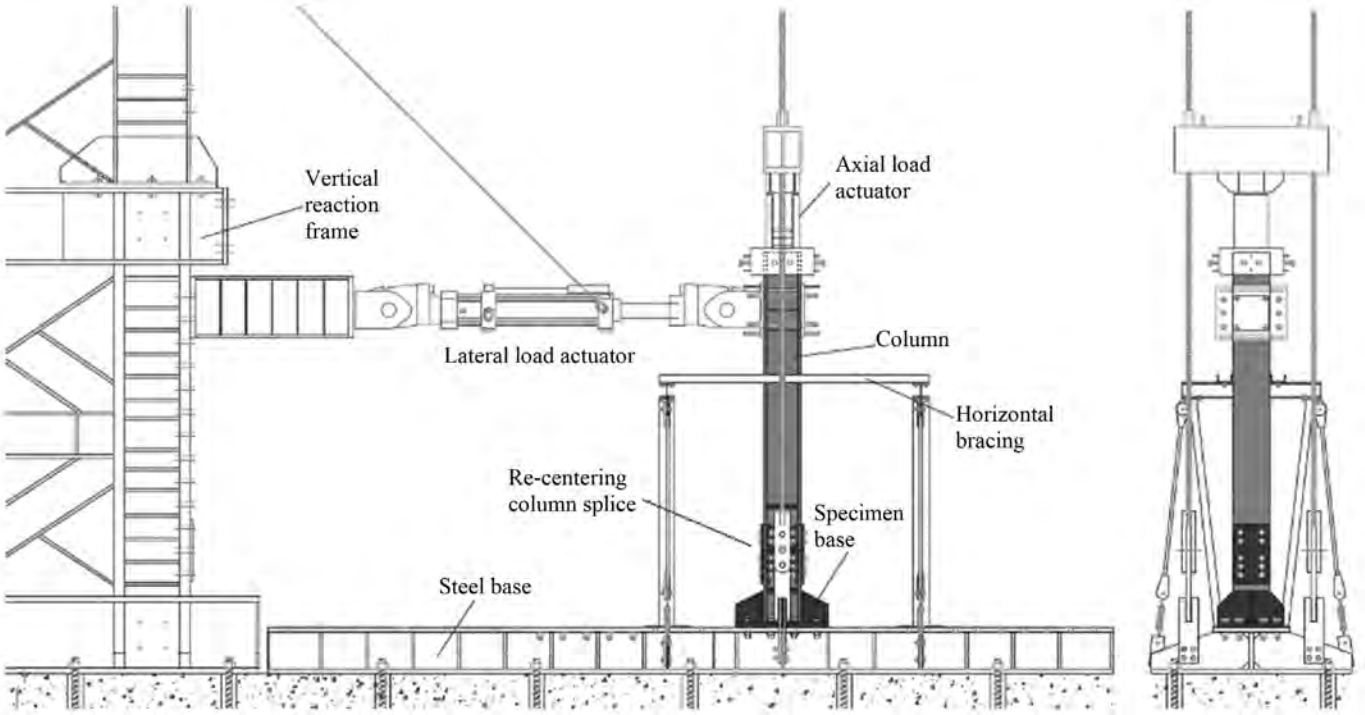

Fig. 4. Front and side views of the test setup.

with the bars. The test specimens with 12.5% axial load ratio exhibited much higher residual rotations. The recentering bars reduced the residual rotations from almost 50 mrad to 31 mrad. However, higher-capacity bars were needed to provide recentering behavior. Additional details for the cyclic tests can be found in Latour et al. (2019).

Pseudo-Dynamic Testing

The proposed self-centering column base connection was further validated with pseudo-dynamic tests. For a more realistic dynamic-response history, a computer simulation was used to account for damping and inertial effects, and the physical test provided restoring force and displacement data for the structure. The structure was idealized as a discrete-parameter system with one degree of freedom. With this idealization, the pseudo-dynamic tests could be conducted with the same test setup used for the cyclic testing. Two ground motions, Kobe (Japan, 1995) and Spitak (Armenia, 1988), were selected to compare results for ground motions with different characteristics. "Kobe is a seismic event inducing a high number of large amplitude cycles, Spitak is characterized mainly by two large reversal and many low amplitude cycles. The scale factor of the seismic events was selected in order to achieve in the connection, approximately, a rotation of 40 mrad" (Latour et al., 2019). An axial load ratio of 25% was used for all tests. Specimens with and without the recentering bars were tested for the Kobe ground motion. The results for the Kobe tests [scale factor 1.4 (PGA = 0.35g)] will be briefly presented. Results for the Spitak test can be found in Latour et al. (2019).

The pseudo-dynamic test results highlighted the role of the recentering bars. Figure 7 shows the moment-rotation responses for the Kobe ground motion and the improvement in the self-centering behavior of the column base with the recentering bars. The bars reportedly reduced the residual rotation from 5.2 mrad to 1.7 mrad. The improved self-centering behavior can also be seen in the reduction of residual drift in the displacement time history plots in Figure 8.

NUMERICAL SIMULATIONS

The proposed self-centering column base connection was further investigated through numerical time-history analyses of moment-resisting frames. Two four-bay, six-story MRFs were designed, one with conventional, fixed column bases and one with self-centering connections. The MRFs had 20-ft bays and 10.5-ft story heights with the exception of the 11.5-ft first story. Preliminary beam sizing was based on dead and live loads of 84 psf and 42 psf. The MRF members were designed for a region of high seismicity (PGA = 0.35g) and dense sand, gravel, or stiff clay.

The self-centering column base connections were represented with a mechanical model, an assembly of springs and gap elements. The mechanical model was able to capture the moment-rotation responses from the experimental tests. Four bilinear springs in parallel with gap elements simulated the hysteretic response of the friction dampers.

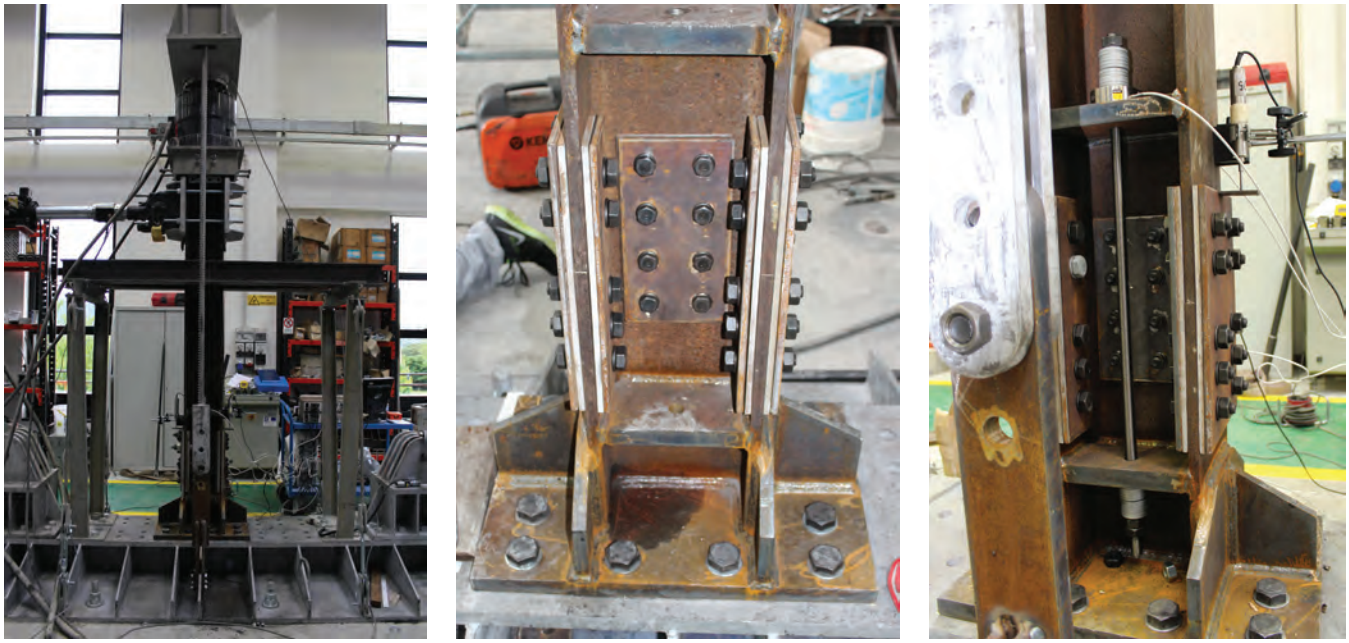

(a) *(b)* *(c)*

Fig. 5. (a) Test setup; (b) connection being assembled; (c) column base connection.

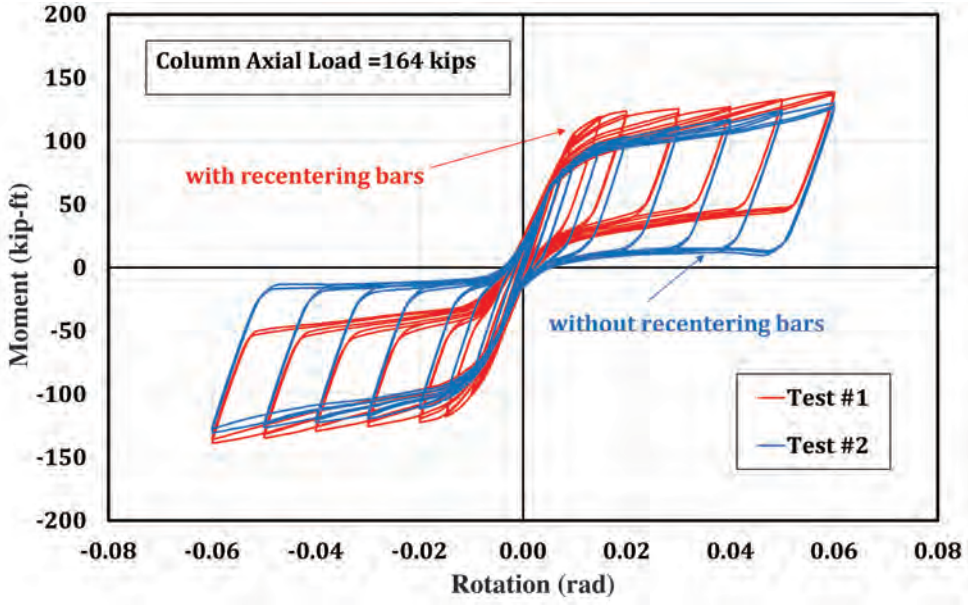

(a) 25% axial load ratio

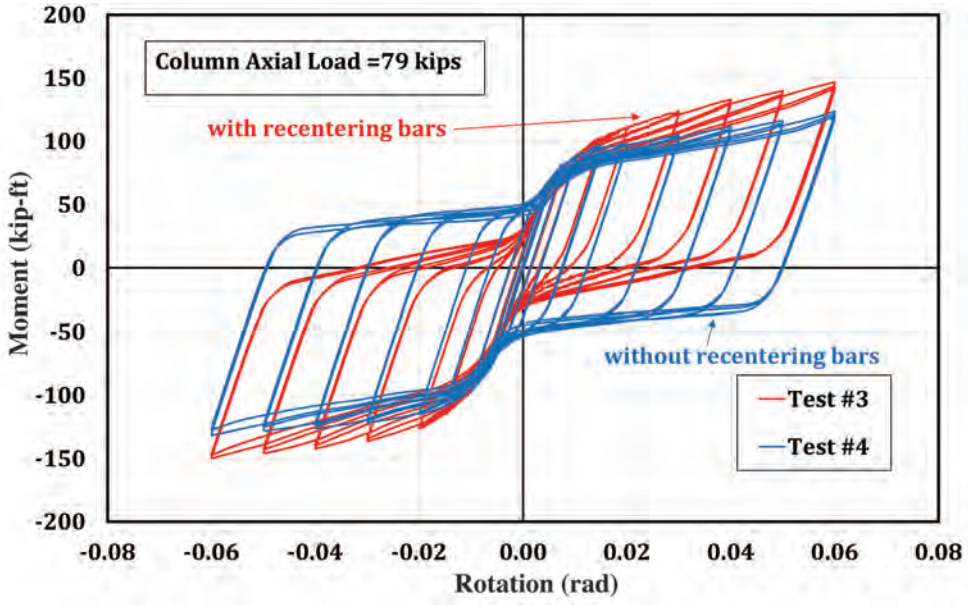

(b) 12.5% axial load ratio

Fig. 6. Moment-rotation responses.

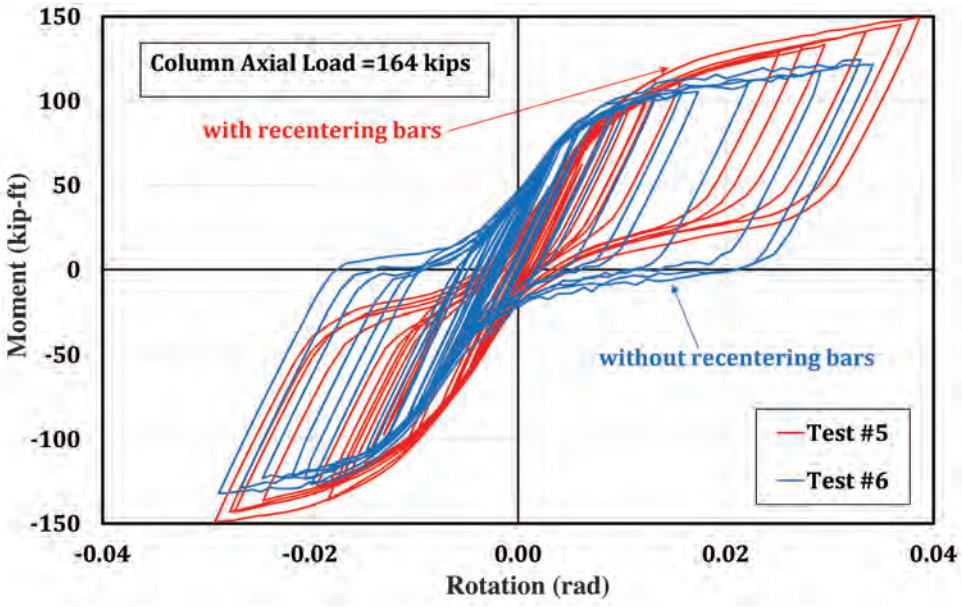

Fig. 7. Moment-rotation responses for the Kobe ground motion.

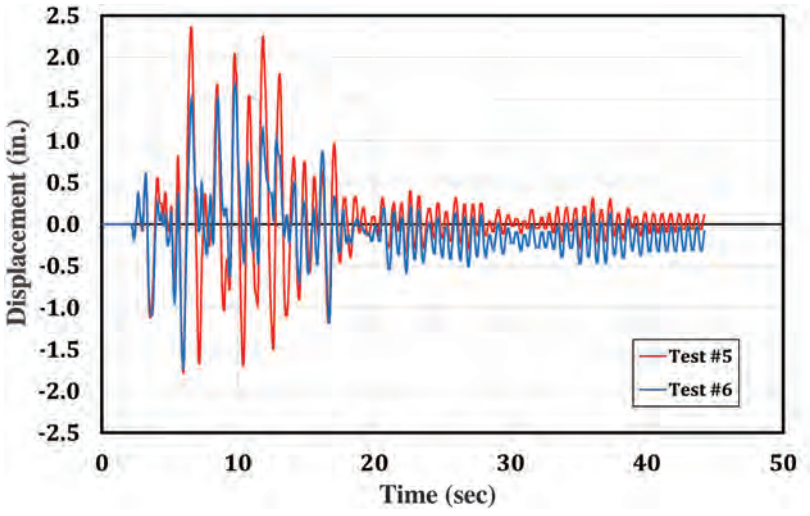

Fig. 8. Displacement time histories for Kobe ground motion.

A central bilinear spring simulated the initial prestress and the hysteretic response of the recentering bars. Properties of the springs were calibrated to the experimental data. Meanwhile, the bolted beam-to-column connections with friction dampers (Figure 1) were modeled according to Latour et al. (2018). A damping ratio of 5% was used.

The time-history analyses were conducted for a simulated seismic event. That simulated event was based on eight natural ground motions. Figure 9 compares the roof displacement time histories for the conventional and self-centering column base MRFs. For the conventional full-strength column base connections, the residual roof displacement at the top of the building was 13.8 in., corresponding to 18 mrad of drift. Use of self-centering column base connections reduced the residual displacement by 85%, to 2.4 in., or 3 mrad drift, well within acceptable levels.

SUMMARY AND FUTURE WORK

The Salerno-Coimbra team has proposed a self-centering column base connection designed to minimize initial costs and economic losses. The proposed connection is a column-splice with friction pads and threaded bars with Belleville disk springs, located just above a traditional full-strength base plate connection. With the self-centering column base connection, damage and residual drifts are limited, and the connection components are expected to be easy to repair or replace if needed. The self-centering column base has been validated through quasi-static cyclic testing and pseudo-dynamic testing. The self-centering connection was further investigated through numerical time-history analyses of moment resisting frame (MRFs) comparing conventional, fixed column bases to self-centering column bases. The experimental and numerical results are promising. The research team looks to extend the work to other configurations to more broadly validate their self-centering column base concept.

ACKNOWLEDGMENTS

Special thanks to Professor Aldina Santiago for all of the materials, coordination, edits, and other feedback and contributions. The work of the entire research team, including graduate research assistants, is appreciated.

The researchers would like to gratefully acknowledge the sponsorship from the European Commission within RFCS Research & Innovation by research grant RFSR-CT-2015-00022. Any findings, recommendations, or other material within are those of the researchers and do not necessarily reflect the views of the sponsors.

REFERENCES

Borzouie, J., MacRae, G.A., Chase, J.G., Rodgers, G.W., and Clifton, G.C. (2015), "Column Base Weak Axis Aligned Asymmetric Friction Connection Cyclic Performance," *Proceedings of the 8th International Conference on Behavior of Steel Structures in Seismic Areas*, Shanghai, China, July 1–3.

Chen, C.C., Lin, H.-W., and Tsai, R.-S. (2014), "Self-Centering and Energy Dissipation of a Post-Tensioned Steel Column Base," *Proceedings of the Second European Conference on Earthquake Engineering and Seismology*, pp. 25–29.

Chi, H. and Liu, J. (2012), "Seismic Behavior of Post-Tensioned Column Base for Steel Self-Centering Moment Resisting Frame," *Journal of Constructional Steel Research*, Vol. 78, pp. 117–130, https://doi.org/10.1016/j.jcsr.2012.07.005.

Eatherton, M.R., Ma., X., Krawinkler, H., Mar, D., Billington, S., Hajjar, J.F., and Deierlein, G.G. (2014), "Design Concepts for Controlled Rocking of Self-Centering Steel-Braced Frames," *Journal of Structural Engineering,* Vol. 140, No. 11, https://doi.org/10.1061/(ASCE)ST.1943-541X.0001047.

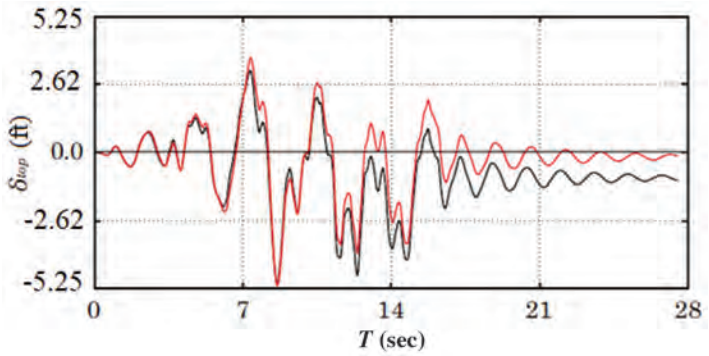

Fig. 9. Roof displacement time histories for simulated ground motion.

Freddi, F., Dimopoulos, C.A., and Karavasilis, T.L. (2017), "Rocking Damage-Free Steel Column Base with Friction Devices: Design Procedure and Numerical Evaluation," *Earthquake Engineering & Structural Dynamics*, 10.1002/eqe.2904.

Gledhill, S.M., Sidwell, G.K., and Bell, D.K. (2008), "The Damage Avoidance Design of Tall Steel Frame Buildings—Fairlie Terrace Student Accommodation Project," *Proceedings of the NZSEE Conference*, Victoria University of Wellington, New Zealand.

Grigorian, C.E., Yang, T.S., and Popov, E.P. (1993), "Slotted Bolted Connection Energy Dissipators," *Earthquake Spectra*, Vol. 9, No. 3, pp. 491–504.

Hayashi, K., Skalomenos, K., Inamasu, H., and Luo, Y.-B. (2018), "Self-Centering Rocking Composite Frame Using Double-Skin Concrete-Filled Steel Tube Columns and Energy-Dissipating Fuses in Multiple Locations," *Journal of Structural Engineering*, ASCE, Vol. 144, No. 9, https://doi.org/10.1061/(ASCE)ST.1943-541X.0002157.

Kamperidis, V., Karavasilis, T.L., and Vasdravellis, G. (2018), "Self-Centering Steel Column Base with Metallic Energy Dissipation Devices," *Journal of Constructional Steel Research*, Vol. 149, pp. 14–30, https://doi.org/10.1016/j.jcsr.2018.06.027.

Khoo, H., Clifton, C. Butterworth, J. MacRae, G., and Ferguson, G. (2012), "Influence of Steel Shim Hardness on the Sliding Hinge Joint Performance," *Journal of Constructional Steel Research*, Vol. 72, pp. 119–129.

Latour, M., D'Aniello, M., Zimbru, M., Rizzano, G., Piluso, V., and Landolfo, R. (2018), "Removable Friction Dampers for Low-Damage Steel Beam-to-Column Joints," *Soil Dynamics and Earthquake Engineering*, Vol. 115, pp. 66–81.

Latour, M., Rizzano, G., Santiago, A., and Simoes da Silva, L. (2019), "Experimental Response of a Low-Yielding, Self-Centering, Rocking Column Base Joint with Friction Dampers," *Soil Dynamics and Earthquake Engineering*, Vol. 116, pp. 580–592, https://doi.org/10.1016/j.soildyn.2018.10.011.

MacRae, G.A., Urmson, C.R., Walpole, W.R., Moss, P., Hyde K., and Clifton, C. (2009), "Axial Shortening of Steel Columns in Buildings Subjected to Earthquakes," *Bulletin NZSEE*, Vol. 42, p. 275.

Ramhormozian S., Clifton G.C., and MacRae G.A. (2014), "The Asymmetric Friction Connection with Belleville Springs in the Sliding Hinge Joint," *Proceedings of the NZSEE Conference*, Auckland, New Zealand.

Sause, R., Ricles, J., Lin, Y.-C., Seo, C.-Y., Roke, D., and Chancellor, B. (2010), "Self-Centering Damage-Free Seismic-Resistant Steel Frame Systems," *2010 Joint Conference Proceedings—Seventh International Conference on Urban Earthquake Engineering and Fifth International Conference on Earthquake Engineering*, Tokyo, Japan, February.

Silva, L. (2016), "Design of a 'Free from Damage' Column Base Connection for Seismic Actions," Master in Civil Engineering Thesis, University of Coimbra, Portugal.

Wang, X.-T., Xie, C.-D., Lin, L.-H., and Li, J. (2019), "Seismic Behavior of Self-Centering Concrete-Filled Square Steel Tubular (CFST) Column Base," *Journal of Constructional Steel Research*, Vol. 156, pp. 75–85, https://doi.org/10.1016/j.jcsr.2019.01.025.

Wiebe, L., Christopoulos, C., Tremblay, R., and Leclerc, M. (2013), "Mechanisms to Limit Higher Mode Effects in a Controlled Rocking Steel Frame 2: Large-Amplitude Shake Table Testing," *Earthquake Engineering & Structural Dynamics*, Vol. 42, No. 7, June, pp. 1,069–1,086, https://doi.org/10.1002/eqe.2258.

Guide for Authors

Scope

Engineering Journal is dedicated to the improvement and advancement of steel construction. Its pages are open to all who wish to report on new developments or techniques in steel design, research, the design and/or construction of new projects, steel fabrication methods, or new products of significance to the uses of steel in construction. Only original papers should be submitted.

General

Papers intended for publication should be submitted by email Margaret Matthew, editor, at **matthew@aisc.org**.

The articles published in the *Engineering Journal* undergo peer review before publication for (1) originality of contribution; (2) technical value to the steel construction community; (3) proper credit to others working in the same area; (4) prior publication of the material; and (5) justification of the conclusion based on the report.

All papers within the scope outlined above will be reviewed by engineers selected from among AISC, industry, design firms, and universities. The standard review process includes outside review by an average of three reviewers, who are experts in their respective technical area, and volunteers in the program. Papers not accepted will not be returned to the author. Published papers become the property of the American Institute of Steel Construction and are protected by appropriate copyrights. No proofs will be sent to authors. Each author receives three copies of the issue in which his contribution appears.

Manuscripts

Manuscripts must be provided in Microsoft Word format. Include a PDF with your submittal so we may verify fonts, equations and figures. View our complete author guidelines at **aisc.org/ej**.

Smarter. Stronger. Steel.

American Institute of Steel Construction
130 E Randolph St, Ste 2000, Chicago, IL 60601
312.670.2400 | aisc.org/ej